Scalable Molecular Dynamics with NAMD

JAMES C. PHILLIPS,[1] ROSEMARY BRAUN,[1] WEI WANG,[1] JAMES GUMBART,[1]
EMAD TAJKHORSHID,[1] ELIZABETH VILLA,[1] CHRISTOPHE CHIPOT,[2] ROBERT D. SKEEL,[3]
LAXMIKANT KALÉ,[3] KLAUS SCHULTEN[1]

[1]*Beckman Institute, University of Illinois at Urbana–Champaign, Urbana, Illinois 61801*
[2]*UMR CNRS/UHP 7565, Université Henri Poincaré,*
54506 Vandœuvre-lès-Nancy, Cedex, France
[3]*Department of Computer Science and Beckman Institute, University of Illinois at*
Urbana–Champaign, Urbana, Illinois 61801

Abstract: NAMD is a parallel molecular dynamics code designed for high-performance simulation of large biomolecular systems. NAMD scales to hundreds of processors on high-end parallel platforms, as well as tens of processors on low-cost commodity clusters, and also runs on individual desktop and laptop computers. NAMD works with AMBER and CHARMM potential functions, parameters, and file formats. This article, directed to novices as well as experts, first introduces concepts and methods used in the NAMD program, describing the classical molecular dynamics force field, equations of motion, and integration methods along with the efficient electrostatics evaluation algorithms employed and temperature and pressure controls used. Features for steering the simulation across barriers and for calculating both alchemical and conformational free energy differences are presented. The motivations for and a roadmap to the internal design of NAMD, implemented in C++ and based on Charm++ parallel objects, are outlined. The factors affecting the serial and parallel performance of a simulation are discussed. Finally, typical NAMD use is illustrated with representative applications to a small, a medium, and a large biomolecular system, highlighting particular features of NAMD, for example, the Tcl scripting language. The article also provides a list of the key features of NAMD and discusses the benefits of combining NAMD with the molecular graphics/sequence analysis software VMD and the grid computing/collaboratory software BioCoRE. NAMD is distributed free of charge with source code at www.ks.uiuc.edu.

© 2005 Wiley Periodicals, Inc.   J Comput Chem 26: 1781–1802, 2005

Key words: biomolecular simulation; molecular dynamics; parallel computing

Introduction

The life sciences enjoy today an ever-increasing wealth of information on the molecular foundation of living cells as new sequences and atomic resolution structures are deposited in databases. Although originally the domain of experts, sequence data can now be mined with relative ease through advanced bioinformatics and analysis tools. Likewise, the molecular dynamics program NAMD,[1] together with its sister molecular graphics program VMD,[2] seeks to bring easy-to-use tools that mine structure information to all who may benefit, from the computational expert to the laboratory experimentalist.

The increase in our knowledge of structures is not as dramatic as that of sequences, yet the number of newly deposited structures reached a record 5000 last year. For example, the structures of pharmacologically crucial membrane proteins, which were essentially unknown 10 years ago, are being resolved today at a rapid pace. Structures yield static information that can be viewed with molecular graphics software such as VMD. However, structures also hold the key to dynamic information that leads to understanding function and mechanism, intellectual guideposts for basic medical research. With NAMD we want to simplify access to dynamic information extrapolated from structures and provide a molecular modeling tool that can be used productively by a wide

Figure 1. Growth in practical simulation size illustrated by comparison of estrogen receptor DNA-binding domain simulation of ref. 5, left, 36,000 atoms simulated over 100 ps, published in 1997, with multiscale LacI–DNA complex simulation of ref. 6, right, 314,000 atoms simulated over 10 ns, published in 2005 and described in the exemplary applications section. [Color figure can be viewed in the online issue, which is available at www.interscience.wiley.com.]

group of biomedical researchers, including particularly experimentalists.

On a molecular scale, the fundamental processing units in the living cell are often huge in size and function in an even larger complex environment. Striking progress has been achieved in characterizing the immense machines of the cell, such as the ribosome, at the atomic level. Advances in biomedicine demand tools to model these machines to understand their function and their role in maintaining the health of cells. Accordingly, the purpose of NAMD is to enable high-performance classical simulation of biomolecules in realistic environments of 100,000 atoms or more. The progress made in this regard is illustrated in Figure 1. A decade ago in its first release,[3,4] NAMD permitted simulation of a protein–DNA complex encompassing 36,000 atoms,[5] one of the largest simulations carried out at the time. The most recent release permitted the simulation of a protein–DNA complex of 314,000 atoms.[6] To probe the behavior of this 10-fold larger system, the simulated period actually increased 100-fold as well.

The following article on NAMD is directed to novices and experts alike. It explains the concepts and algorithms underlying modern molecular dynamics (MD) simulations as realized in NAMD, for example, the efficient numerical integration of the Newtonian equations of motion, the use of statistical mechanics methods for simulations that control temperature and pressure, the efficient evaluation of electrostatic forces through the particle-mesh Ewald method, the use of steered and interactive MD to manipulate and probe biomolecular systems and to speed up reaction processes, and the calculation of alchemical and conformational free energy differences.

The article describes the design of NAMD and the motivation behind the design, that is, to permit continuous software development in view of ever-changing technologies, to utilize parallel computers of any size effectively via message driven computation, to run well on platforms from laptops and desktops—where NAMD is actually used most—to parallel computers with thou-

sands of processors. The article also demonstrates how the user can readily extend NAMD through the Tcl scripting language and elaborates on the strengths of NAMD in steered and interactive MD.

To demonstrate the broad utility of NAMD, the article introduces three typical applications as they are encountered in modern research, involving a small, an intermediate, and a large biomolecular system. We emphasize which features of NAMD were used and which were most helpful in completing the three modeling projects expeditiously. We also refer readers to tutorial material (available at http://www.ks.uiuc.edu/Training/Tutorials/) that has been proven helpful in NAMD training workshops and university courses. In fact, the first application presented below ubiquitin stems directly from the introductory NAMD tutorial. Other tutorials—for which a laptop provides sufficient computational power—introduce steered MD and simulations of membrane channels, as well as the use of VMD in trajectory analysis.

Finally, a conclusion section summarizes the features of NAMD that have proven to be most relevant to nonexpert as well as expert users and describes the great benefits that NAMD gains from its close link to the widely used molecular graphics program VMD, which permits model building as well as trajectory analysis. The integration of NAMD into the grid software BioCoRE is also mentioned.

Molecular Dynamics Concepts and Algorithms

In this section we outline concepts and algorithms of classical MD simulations. In these simulations the atoms of a biopolymer move according to the Newtonian equations of motion

$$m_\alpha \ddot{\vec{r}}_\alpha = -\frac{\partial}{\partial \vec{r}_\alpha} U_{\text{total}}(\vec{r}_1, \vec{r}_2, \ldots, \vec{r}_N), \quad \alpha = 1, 2 \ldots N, \quad (1)$$

where m_α is the mass of atom α, $\vec{r}_\alpha$ is its position, and U_{total} is the total potential energy that depends on all atomic positions and, thereby, couples the motion of atoms. The potential energy, represented through the MD "force field," is the most crucial part of the simulation because it must faithfully represent the interaction between atoms, yet be cast in the form of a simple mathematical function that can be calculated quickly.

Below we introduce first the functional form of the force field utilized in NAMD. We then comment on the special problem of calculating the Coulomb potential and forces efficiently. The numerical integration of (1) is then explained, followed by an outline of simulation strategies for controlling temperature and pressure. In the case of such simulations, frictional and fluctuating forces are added to (1) following the principles of nonequilibrium statistical mechanics. Finally, we describe how external, user-defined forces are added to simulations to manipulate and probe biomolecular systems.

Force Field Functions

For an all-atom MD simulation, one assumes that every atom experiences a force specified by a model force field accounting for

the interaction of that atom with the rest of the system. Today, such force fields present a good compromise between accuracy and computational efficiency. NAMD employs a common potential energy function that has the following contributions:

$$U_{\text{total}} = U_{\text{bond}} + U_{\text{angle}} + U_{\text{dihedral}} + U_{\text{vdW}} + U_{\text{Coulomb}}. \quad (2)$$

The first three terms describe the stretching, bending, and torsional bonded interactions,

$$U_{\text{bond}} = \sum_{\text{bonds } i} k_i^{\text{bond}}(r_i - r_{0i})^2, \quad (3)$$

$$U_{\text{angle}} = \sum_{\text{angles } i} k_i^{\text{angle}}(\theta_i - \theta_{0i})^2, \quad (4)$$

$$U_{\text{dihedral}} = \sum_{\text{dihedral } i} \begin{cases} k_i^{\text{dihe}}[1 + \cos(n_i \phi_i - \gamma_i)], n_i \neq 0 \\ k_i^{\text{dihe}}(0_i - \gamma_i)^2 \, n = 0, \end{cases} \quad (5)$$

where *bonds* counts each covalent bond in the system, *angles* are the angles between each pair of covalent bonds sharing a single atom at the vertex, and *dihedral* describes atom pairs separated by exactly three covalent bonds with the central bond subject to the torsion angle ϕ (Fig. 2). An "improper" dihedral term governing the geometry of four planar, covalently bonded atoms is also included as depicted in Figure 2.

The final two terms in eq. (2) describe interactions between nonbonded atom pairs:

$$U_{\text{vdW}} = \sum_i \sum_{j>i} 4\varepsilon_{ij} \left[\left(\frac{\sigma_{ij}}{r_{ij}} \right)^{12} - \left(\frac{\sigma_{ij}}{r_{ij}} \right)^6 \right], \quad (6)$$

$$U_{\text{Coulomb}} = \sum_i \sum_{j>i} \frac{q_i q_j}{4\pi\varepsilon_0 r_{ij}}, \quad (7)$$

which correspond to the van der Waal's forces (approximated by a Lennard–Jones 6–12 potential) and electrostatic interactions, respectively.

In addition to the intrinsic potential described by the force field, NAMD also provides the user with the ability to apply external forces to the system. These forces may be used to guide the system into configurations of interest, as in steered and interactive MD (described below).

For every particle in a given context of bonds, the parameters k_i^{bond}, r_{0i}, etc., for the interactions given in eqs. (3)–(5) are laid out in force field parameter files. The determination of these parameters is a significant undertaking generally accomplished through a combination of empirical techniques and quantum mechanical calculations;[7–9] the force field is then tested for fidelity in reproducing the structural, dynamic, and thermodynamic properties of small molecules that have been well-characterized experimentally, as well as for fidelity in reproducing bulk properties. NAMD is able to use the parameterizations from both CHARMM[7] and AMBER[10] force field specifications.
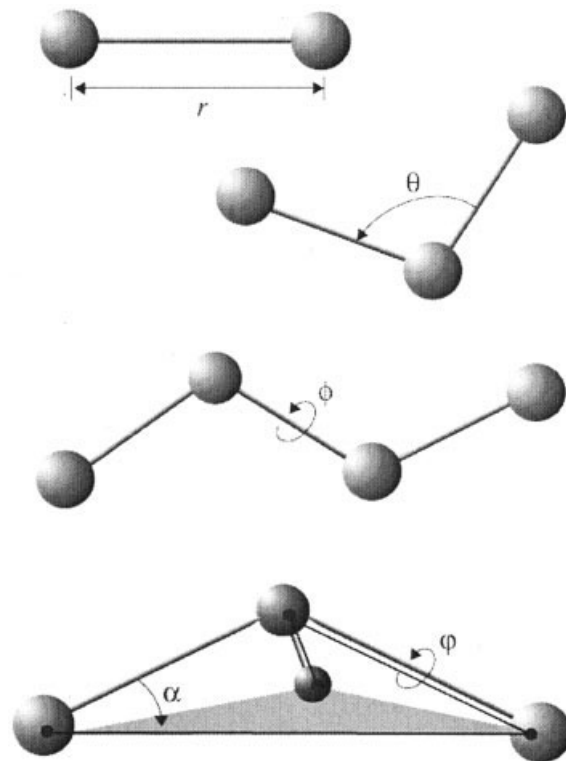

Figure 2. Internal coordinates for bonded interactions: r governs bond stretching; θ represents the bond angle term; ϕ gives the dihedral angle; the small out-of-plane angle α is governed by the so-called "improper" dihedral angle φ.

To avoid surface effects at the boundary of the simulated system, periodic boundary conditions are often used in MD simulations; the particles are enclosed in a cell that is replicated to infinity by periodic translations. A particle that leaves the cell on one side is replaced by a copy entering the cell on the opposite side, and each particle is subject to the potential from all other particles in the system including images in the surrounding cells, thus entirely eliminating surface effects (but not finite-size effects). Because every cell is an identical copy of all the others, all the image particles move together and need only be represented once inside the molecular dynamics code.

However, because the van der Waals and electrostatic interactions [eqs. (6) and (7)] exist between every nonbonded pair of atoms in the system (including those in neighboring cells) computing the long-range interaction exactly is unfeasible. To perform this computation in NAMD, the van der Waals interaction is spatially truncated at a user-specified cutoff distance. For a simulation using periodic boundary conditions, the system periodicity is exploited to compute the full (nontruncated) electrostatic interaction with minimal additional cost using the particle-mesh Ewald (PME) method described in the next section.

Full Electrostatic Computation

Ewald summation[11] is a description of the long-range electrostatic interactions for a spatially limited system with periodic boundary

conditions. The infinite sum of charge-charge interactions for a charge-neutral system is conditionally convergent, meaning that the result of the summation depends on the order in which it is taken. Ewald summation specifies the order as follows:[12] sum over each box first, then sum over spheres of boxes of increasingly larger radii. Ewald summation is considered more reliable than a cutoff scheme,[13–15] although it is noted that the artificial periodicity can lead to bias in free energy,[16,17] and can artificially stabilize a protein that should have unfolded quickly.[18]

Dropping the prefactor $1/4\pi\varepsilon$, the Ewald sum involves the following terms:

$$E_{\text{Ewald}} = E_{\text{dir}} + E_{\text{rec}} + E_{\text{self}} + E_{\text{surface}}, \tag{8}$$

$$E_{\text{dir}} = \frac{1}{2} \sum_{i,j=1}^{N} q_i q_j \sum_{\vec{n}_r}' \frac{\text{erfc}(\beta|\vec{r}_i - \vec{r}_j + \vec{n}_r|)}{|\vec{r}_i - \vec{r}_j + \vec{n}_r|}$$

$$- \sum_{(i,j)\in\text{Excluded}} \frac{q_i q_j}{|\vec{r}_i - \vec{r}_j + \vec{v}_{ij}|}, \tag{9}$$

$$E_{\text{rec}} = \frac{1}{2\pi V} \sum_{\vec{m}\neq 0} \frac{\exp(-\pi^2|\vec{m}|^2/\beta^2)}{|\vec{m}|^2} \left| \sum_{i=1}^{N} q_i \exp(2\pi \text{i} \vec{m} \cdot \vec{r}_i) \right|^2, \tag{10}$$

$$E_{\text{self}} = -\frac{\beta}{\sqrt{\pi}} \sum_{i=1}^{N} q_i^2, \tag{11}$$

$$E_{\text{surface}} = \frac{2\pi}{(2\varepsilon_s + 1)V} \left| \sum_{i=1}^{N} q_i \vec{r}_i \right|^2. \tag{12}$$

Here, q_i and $\vec{r}_i$ are the charge and position of atom i, respectively, and $\vec{n}_r$ is the lattice vector. For an arbitrary simulation box defined by three independent base vectors $\vec{a}_1, \vec{a}_2, \vec{a}_3$, one defines $\vec{n}_r = n_1\vec{a}_1 + n_2\vec{a}_2 + n_3\vec{a}_3$, where n_1, n_2, and n_3 are integers. $\sum'$ denotes a summation over $\vec{n}_r$ that excludes the $\vec{n}_r = 0$ term in the case $i = j$; "excluded" denotes the set of atom pairs whose direct electrostatic interaction should be excluded. $\vec{v}_{ij}$ denotes the lattice vector for the (i, j) pair that minimizes $|\vec{r}_i - \vec{r}_j + \vec{v}_{ij}|$. β is a parameter adjusting the workload distribution for direct and reciprocal sums. ε_s is the dielectric constant of the surroundings of the simulation box, which is water for most biomolecular systems. V is the volume of the simulation box. $\vec{m}$ is the reciprocal vector defined as $\vec{m} = m_1\vec{b}_1 + m_2\vec{b}_2 + m_3\vec{b}_3$, where m_1, m_2, m_3 are integers, and the reciprocal base vectors $\vec{b}_1, \vec{b}_2, \vec{b}_3$ are defined so that

$$\vec{a}_\alpha \cdot \vec{b}_\beta = \delta_{\alpha\beta}, \quad \alpha, \beta = 1, 2, 3. \tag{13}$$

The complementary error function $\text{erfc}(x)$ in eq. (9) is

$$\text{erfc}(x) = \frac{2}{\sqrt{\pi}} \int_x^\infty e^{-t^2} dt. \tag{14}$$

The Ewald sum in eq. (8) has four terms: direct sum E_{dir}, reciprocal sum E_{rec}, self-energy E_{self}, and surface energy E_{surface}. The self-energy term is a trivial constant, while the surface term is usually neglected by assuming the "tin-foil" boundary condition $\varepsilon_s = \infty$, which is partly due to the dielectric constant of water ($\varepsilon_s \approx 80$) being much larger than 1. The Ewald sum has a freely chosen parameter β, which can shift the computational load between the direct sum and the reciprocal sum. For a given accuracy, the computationally optimal choice of the parameter leads to a cost proportional to $N^{3/2}$ in the standard computation, where N is the number of charges in the system.[19]

The particle–mesh Ewald (PME)[20] method is a fast numerical method to compute the Ewald sum. NAMD uses the smooth PME (SPME)[21] method for full electrostatic computations. The cost of PME is proportional to $N \log N$ and the time reduction is significant even for a small system of several hundred atoms. In PME, the parameter β is chosen so that the major work load is put into the reciprocal sum while the direct sum is computed by a cost proportional to N only. The reciprocal sum is then computed via fast Fourier transform (FFT) after an approximation is made to delegate the computation to a grid scheme. For this purpose, PME uses an interpolation scheme to distribute the charges, sitting anywhere in real space, to the nodes of a uniform grid as illustrated in Figure 3. SPME uses B-spline functions as the basis functions for the interpolation. The continuity of B-spline functions and their derivatives makes the analytical expression of forces easy to obtain, and reduces the number of FFTs by half compared to the original PME method. In SPME, approximations are made to the potential only; the force is still the exact derivative of the approximated potential. The strict conservation of energy resulting from the computed force is crucial and is strongly assisted by maintaining the symplecticness of the integrator,[22] as discussed further below.

The PME method can be adopted to compute the electrostatic potential in real space and has been implemented in VMD (see Fig. 4). The feature has been used recently in a ground-breaking simulation to compute transmembrane electrostatic potentials averaged over an MD trajectory.[23] This feature makes it possible today to compute average electrostatic potentials from first principles and to replace previously used heuristic potentials like those derived from Poisson–Boltzmann theory.

The PME method does not conserve energy and momentum simultaneously, but neither does the particle-particle/particle-mesh method[24] or the multilevel summation method.[25,26] Momentum conservation can be enforced by subtracting the net force from the reciprocal sum computation, albeit at the cost of a small long-time energy drift.

Numerical Integration

Biomolecular simulations often require millions of time steps. Furthermore, biological systems are *chaotic;* trajectories starting from slightly different initial conditions diverge exponentially fast and after a few picoseconds are completely uncorrelated. However, highly accurate trajectories is not normally a goal for biomolecular simulations; more important is a proper sampling of phase space. Therefore, for constant energy (NVE ensemble) simulations, the key features of an integrator are not
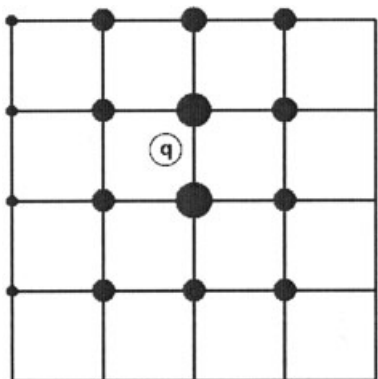
Figure 3. In PME, a charge (denoted by an empty circle with label "q" in the figure) is distributed over grid (here a mesh in two dimensions) points with weighting functions chosen according to the distance of the respective grid points to the location of the charge. Positioning all charges on a grid enables the application of the FFT method and significantly reduces the computation time. In real applications, the grid is three-dimensional.

only how accurate it is locally, but also how efficient it is, and how well it preserves the fundamental dynamical properties, such as energy, momentum, time-reversibility, and symplecticness.

The time evolution of a strict Hamiltonian system is symplectic.[22] A consequence of this is the conservation of phase space volume along the trajectory, that is, the enforcement of the Liouville theorem (ref. 27, p. 69). To a large extent, the trajectories computed by numerical integrators observing symplecticness represent the solution of a closely related problem that is still Hamiltonian.[28] Because of this, the errors, unavoidably generated by an integrator at each time step, accumulate imperceptibly slowly, resulting in a very small long-time energy drift, if there is any at all (ref. 22, theorem IX.8.1). Artificial measures to conserve energy, for example, scaling the velocity at each time step so that the total energy is constant, lead to biased phase space sampling of the constant energy surface;[29] in contrast, there has been no evidence that symplectic integrators have this problem.

A simple example demonstrates the merit of a symplectic integrator. For this purpose, the one-dimensional harmonic oscillator problem has been numerically integrated, the resulting trajectory being shown in Figure 5. We note that the comparison is "unfair" to the symplectic method with respect to both accuracy (Δt^2 local error for the symplectic method vs. Δt^5 for the Runge–Kutta method, where Δt is the time step), and computational effort (single force evaluation per time step for the symplectic method vs. four force evaluations for the Runge–Kutta method). Nevertheless, the symplectic method shows superior long-time stability.

NAMD uses the Verlet method (ref. 31, section 4.2.3) for NVE ensemble simulations. The "velocity-Verlet" method obtains the position and velocity at the next time step (r_{n+1}, v_{n+1}) from the current one (r_n, v_n), assuming the force $F_n = F(r_n)$ is already computed, in the following way:

$$\text{"half-kick"} \quad v_{n+1/2} = v_n + M^{-1}F_n \cdot \Delta t/2,$$

$$\text{"drift"} \quad r_{n+1} = r_n + v_{n+1/2}\Delta t,$$

$$\text{"compute force"} \quad F_{n+1} = F(r_{n+1}),$$

$$\text{"half-kick"} \quad v_{n+1} = v_{n+1/2} + M^{-1}F_{n+1} \cdot \Delta t/2.$$

Here, M is the mass. The Verlet method is symplectic and time reversible, conserves linear and angular momentum, and requires only one force evaluation for each time step. For a fixed time period, the method exhibits a (global) error proportional to Δt^2.

More accurate (higher order) methods are desirable if they can increase the time step per force evaluation. Higher order Runge–Kutta type methods, symplectic or not, are not suitable for biomolecular simulations because they require several force evaluations for each time step and force evaluation is by far the most time-consuming task in molecular dynamics simulations. Gear type predictor–corrector methods,[32] or linear multistep methods in general, are not symplectic (ref. 22, theorem XIV.3.1). No symplectic method has been found as yet that is both more accurate than the Verlet method and as practical for biomolecular simulations.

NAMD employs a multiple-time-stepping[13,33,34] method to improve integration efficiency. Because the biomolecular interactions collected in eq. (2) generally give rise to several different time scales characteristic for biomolecular dynamics, it is natural to compute the slower-varying forces less frequently than faster varying ones in molecular dynamics simulations. This idea is implemented in NAMD by three levels of integration loops. The inner loop uses only bonded forces to advance the system, the middle loop uses Lennard–Jones and short-range electrostatic forces, and the outer loop uses long-range electrostatic forces. We note that the method implemented in NAMD is symplectic and time reversible.

The longest time step for the multiple time-stepping method is limited by resonance.[35] When good energy conservation is needed for NVE ensemble simulations we recommend choosing 2 fs, 2 fs, and 4 fs as the inner, middle, and outer time steps if rigid bonds to hydrogen atoms are used; or 1 fs, 1 fs, and 3 fs if bonds to
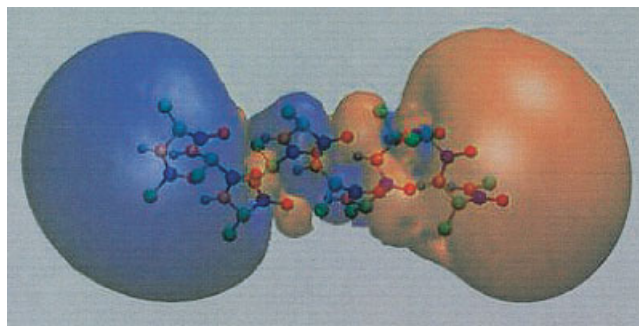

Figure 4. Smoothed electrostatic potential of decalanine in vacuum as calculated with the PME plugin of VMD. Atoms are colored by charge (blue is positive, red is negative). The helix dipole is clearly visible from the two potential isosurfaces $+20k_BT/e$ (blue, left lobe) and $-20k_BT/e$ (red, right lobe). [Color figure can be viewed in the online issue, which is available at www.interscience.wiley.com.]
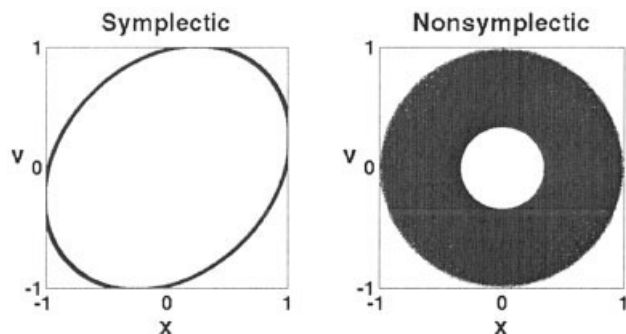
Figure 5. A symplectic method demonstrates superior long-time stability: the symplectic method used here is the symplectic Euler method ([22], Theorem 3.3), whose local error is proportional to Δt^2; the nonsymplectic method used is the Runge–Kutta method ([30], sect. 8.3.3) whose local error is proportional to Δt^5. The system described is a one-dimension harmonic oscillator. The equation of motion is $m\ddot{x} = -m\omega^2 x$, with $m = \omega = 1$, and initial conditions $x = 1$, $v = 0$. The exact trajectory is the unit circle. The chosen time step is $\Delta t = 0.5$ and 10,000 steps were integrated. The trajectory of the Runge–Kutta method collapses toward the center while the symplectic Euler method maintains a stable orbit even though its trajectory is deformed into an ellipse by a larger local error.

hydrogen are flexible.[36] More aggressive time steps may be used for NVT or NPT ensemble simulations, for example, 2 fs, 2 fs, and 6 fs with rigid bonds and 1 fs, 2 fs, and 4 fs without. Using multiple time stepping can increase computational efficiency by a factor of 2.

NVT and NPT Ensemble Simulations

A fundamental requirement for an integrator is to generate the correct ensemble distribution for the specified temperature and pressure in an appropriate way. For this purpose the Newtonian equations of motion (1) should be modified "mildly" so that the computed short-time trajectory can still be interpreted in a conventional way. To generate the correct ensemble distribution, the system is coupled to a reservoir, with the coupling being either deterministic or stochastic. Deterministic couplings generally have some conserved quantities (similar to total energy), the monitoring of which can provide some confidence in the simulation. NAMD uses a stochastic coupling approach because it is easier to implement and the friction terms tend to enhance the dynamical stability.

The (stochastic) Langevin equation[37] is used in NAMD to generate the Boltzmann distribution for canonical (NVT) ensemble simulations. The generic Langevin equation is

$$M\dot{v} = F(r) - \gamma v + \sqrt{\frac{2\gamma k_B T}{M}}\, R(t), \quad (15)$$

where M is the mass, $v = \dot{r}$ is the velocity, F is the force, r is the position, γ is the friction coefficient, k_B is the Boltzmann constant, T is the temperature, and $R(t)$ is a univariate Gaussian random process. Coupling to the reservoir is modeled by adding the fluctuating (the last term) and dissipative ($-\gamma v$ term) forces to the

Newtonian equations of motion (1). To integrate the Langevin equation, NAMD uses the Brünger–Brooks–Karplus (BBK) method,[38] a natural extension of the Verlet method for the Langevin equation. The position recurrence relation of the BBK method is

$$r_{n+1} = r_n + \frac{1 - \gamma \Delta t/2}{1 + \gamma \Delta t/2}(r_n - r_{n-1})$$

$$+ \frac{1}{1 + \gamma \Delta t/2}\Delta t^2\left[M^{-1}F(r_n) + \sqrt{\frac{2\gamma k_B T}{\Delta M}}\, Z_n\right], \quad (16)$$

where Z_n is a set of Gaussian random variables of zero mean and variance 1. The BBK integrator requires only one random number for each degree of freedom. The steady-state distribution generated by the BBK method has an error proportional to Δt^2,[39] although the error in the time correlation function can have an error proportional to Δt.[40]

For stochastic equations of motion, position and velocity become random variables while the time evolution of the corresponding probability distribution function is described by the Fokker–Planck equation (ref. 37, section 2.4), a deterministic partial differential equation. The stochastic equations of motion are designed so that the time-independent solution to the Fokker–Planck equation is the targeted ensemble distribution. The relationship between the Langevin equation and the associated Fokker–Planck equation has been invoked, for example, in ref. 41. The theory behind deterministic coupling methods is similar, with the Liouville equation playing the pivotal role.[42]

For NPT ensemble simulations, one of the authors (J.P.) proposed a new set of equations of motion and implemented a numerical integrator in NAMD (ref. 43, pressure control section). It was inspired by the Langevin-piston method[44] and Hoover's method[45–47] for constant pressure simulations. A recent work proposed essentially the same set of equations [the "Langevin–Hoover" method given by eqs. (5a)–(5d) in ref. 48], and proved that they generate the correct ensemble distribution. The only difference between the two is the term $1 + d/N_f$ in eq. (5b) and (5d) of ref. 48, where d is the dimension (generally 3), and N_f is the number of degrees of freedom. The term d/N_f is negligible for most purposes.

Steered and Interactive Molecular Dynamics

Biologically important events often involve transitions from one equilibrium state to another, such as the binding or dissociation of a ligand. However, processes involving the rare event of barrier crossing are difficult to reproduce on MD time scales, which today are still confined to the order of tens of nanoseconds. To address this issue, the application of external forces may be used to guide the system from one state to another, enhancing sampling along the pathway of interest. Recent applications of single-molecule experimental techniques (such as atomic force microscopy and optical tweezers) have enhanced our understanding of the mechanical properties of biopolymers. Steered molecular dynamics (SMD) is the *in silico* complement of such studies, in which external forces are applied to molecules in a simulation to probe their mechanical properties as well as to accelerate processes that are otherwise too slow to model. This method has been reviewed in refs. 49–51.

With advances in available computer power, steering forces can also be applied interactively, instead of in batch mode; we call this technique Interactive Molecular Dynamics (IMD).[52,53] External forces have been applied using NAMD in a variety of ways to a diverse set of systems, yielding new information about the mechanics of proteins,[54] for instance in refs. 6, 55–67 and other studies reviewed in ref. 51. We expect that most molecular dynamics simulations in the future will be of the steered type. This expectation stems from an analogy to experimental biophysics: although many experiments provide unaltered images of biological systems, more experiments investigate systems through well-designed perturbations by physical or chemical means.

SMD

Steered MD may be carried out with either a constant force applied to an atom (or set of atoms) or by attaching a harmonic (spring-like) restraint to one or more atoms in the system and then varying either the stiffness of the restraint[67] or the position of the restraint[68–70] to pull the atoms along. Other external forces or potentials can also be used, such as constant forces or torques applied to parts of the system to induce rotational motion of its domains. NAMD provides built-in facilities for applying a variety of external forces, including the automated application of moving constraints. In SMD, the direction of the applied force is chosen in advance, specified through a few simple lines in an NAMD configuration file. More flexible force schemes can be realized within NAMD through scripting.

As a computational technique, SMD bears similarities to the method of umbrella sampling,[71,72] which also seeks to improve the sampling of a particular degree of freedom in a biomolecular system; however, while umbrella sampling requires a series of equilibrium simulations, SMD simulations apply a constant or time-varying force that results in significant deviations from equilibrium. In consequence, the results of the SMD dynamics have to be analyzed from an explicitly nonequilibrium viewpoint.[54] SMD also permits new types of simulations that are more naturally performed and understood as out-of-equilibrium processes.

In constant-force SMD, the atoms to which the force is applied are subject to a fixed, constant force in addition to the force field potential. The affected atoms are specified through a flag in the molecular coordinates (PDB) file, and the force vector is specified in the NAMD configuration. Intermediates found through constant-force SMD simulations may be modeled using the theory of mean first passage times for a barrier-crossing event.[73,74] Typical applied forces range from tens to a thousand picoNewtons (pN).[75]

Constant velocity SMD simulates the action of a moving AFM cantilever on a protein. An atom of the protein, or the center of mass of a group of atoms, is harmonically restrained to a point in space that is then shifted in a chosen direction at a predetermined constant velocity, forcing the restrained atoms to follow (Fig. 6). By default, the SMD harmonic restraint in NAMD only applies along the direction of motion of the restraint point, such that the atoms are unrestrained along orthogonal vectors; it is possible, however, to apply additional restraints. As with constant force SMD, the affected atoms are specified through a flag in the PDB file; the force constant of the restraint and the velocity of the restraint point are specified in the NAMD configuration file. For a group of atoms harmonically restrained with a force constant k moving with velocity v in the direction $\vec{n}$, the additional potential

$$\Delta U(\vec{r}_1, \vec{r}_2, \ldots, t) = \frac{1}{2} k[vt - (\vec{R}(t) - \vec{R}_0) \cdot \vec{n}]^2 \qquad (17)$$

is applied, where $\vec{R}(t)$ is the current center of mass of the SMD atoms and $\vec{R}_0$ is their initial center of mass. $\vec{n}$ is a unit vector. In AFM experiments, the spring constants k of the cantilevers are typically of the order of 1 pN/Å, so that thermal fluctuations in the position of an attached ligand, $(k_B T/k)^{1/2}$, are large on the atomic scale, for example, 6 Å. However, in SMD simulations stiffer springs ($k \sim 70$ pN/Å) are employed, leading to more detailed information about interaction energies as well as finer spatial resolution. However, due to limitations in attainable computational speeds, simulations cover time scales that are typically 10^5 times shorter than those of AFM experiments, necessitating high pulling velocities on the order of 1 Å/ps. As a result, a large amount of irreversible work is performed during SMD simulations, which needs to be discounted to obtain equilibrium information.

A proof that equilibrium properties of a system can be deduced from nonequilibrium simulations was given by Jarzynski.[76,77] The second law of thermodynamics states that the average work $\langle W \rangle$ done through a nonequilibrium process that changes a parameter λ of a system from λ_0 at time zero to λ_t at time t is greater than or equal to the equilibrium free energy difference between the two states specified through the final and initial values of λ:

$$\Delta F = F(\lambda_t) - F(\lambda_0) \leq \langle W \rangle, \qquad (18)$$

where the equality holds only if the process is quasi-static. Jarzynski[76] discovered an equality that holds regardless of the speed of the process:

$$e^{-\beta \Delta F} = \langle e^{-\beta W} \rangle, \qquad (19)$$

where $\beta = (k_B T)^{-1}$. The Jarzynski equality provides a way to extract equilibrium information, such as free energy differences, from averaging over nonequilibrium processes,[76] a method that has been tested against computer simulations[77] and experiments.[78]

A major difficulty that arises with the application of eq. (19) is that the average of exponential work appearing in Jarzynski's equality is dominated by trajectories corresponding to small work values that arise only rarely. Hence, an accurate estimate of free energy requires suitable sampling of such rare trajectories, and thus the accuracy of the method is limited by statistical error. Cumulant expansions[41,62,76,79] are an effective approximation for the exponential average; because the lower order terms of the expansion are less influenced by statistical error, the systematic error introduced by truncating the higher order terms may be considerably smaller than the statistical error that which would be introduced by including them. It can be shown[41] that in the relevant regime of steering by means of stiff springs, the work on the system is Gaussian-distributed regardless of the speed of the process simulated and the cumulant expansion of Jarzynski's equality can safely be terminated at second order.[80]
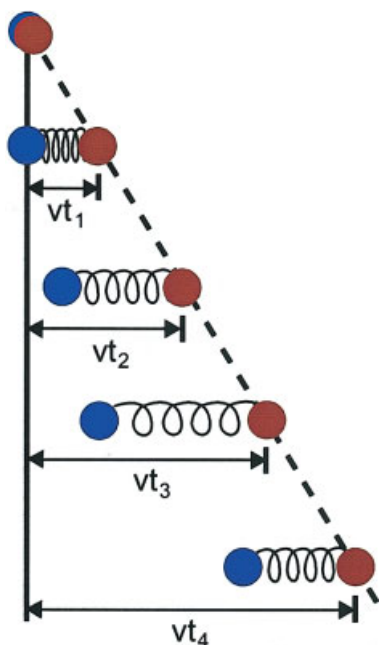
Figure 6. Constant velocity pulling in a one-dimensional case. The dummy atom is colored red, and the SMD atom blue. As the dummy atom moves at constant velocity, the SMD atom experiences a force that depends linearly on the distance between both atoms. [Color figure can be viewed in the online issue, which is available at www. interscience.wiley.com.]

Application of the Jarzynski identity is comparable in efficiency to the umbrella sampling method.[81] However, the analysis involved in the SMD method is simpler than that involved in umbrella sampling in which one needs to solve coupled nonlinear equations for the weighted histogram analysis method.[31,54,82,83] In addition, the application of the Jarzynski identity has the advantage of uniform sampling of a reaction coordinate. Whereas in umbrella sampling a reaction coordinate is locally sampled nonuniformly proportional to the Boltzmann weight, in SMD a reaction coordinate follows a guiding potential that moves with a constant velocity and, hence, is sampled almost uniformly (computing time is uniformly distributed over the given region of the reaction coordinate). This is particularly beneficial when the potential of mean force (essentially, the free energy profile along the reaction coordinate) contains narrow barrier regions as in ref. 62. In such cases, a successful application of umbrella sampling depends on an optimal choice of biasing potentials, whereas nonequilibrium thermodynamic integration appears to be more robust.[31] However, umbrella sampling is a general method that can be applied to a variety of reaction coordinates, including complex ones like those involved in large conformational changes in proteins.[84]

NAMD also provides the facility for the user to apply other types of external forces to a system. In a technique related to SMD, torques may be applied to induce the rotation of a protein domain. As with SMD, this is implemented in NAMD through a simple specification in the configuration file and does not require additional programming on the part of the researcher. This technique has already been successfully used to study the rotation of the Fo

domain of ATPase.[85] The application of more sophisticated external forces are readily implemented through the NAMD "Tcl forces" interface, which allows the user to specify position- and time-dependent forces to be computed at each time step. This technique has recently been used to mimic the effect of membrane surface tension on a mechanosensitive channel[59] and to model the interaction of the *lac* repressor protein (modeled in atomic-level detail) with DNA described by an elastic rod that exerts forces on the protein.[6,86]

IMD

By using NAMD in conjunction with the molecular graphics software VMD, steering forces can be applied in an interactive manner, rather than only in batch mode.[52] For this purpose, VMD is linked to a NAMD simulation running on the same machine or a remote cluster. This arrangement permits an investigator to view a running simulation and to apply forces based on real-time information about the progress of the simulation (such as visual information or force feedback through a haptic device). The researcher is then able to explore the mechanical properties of the system in a direct, hands-on manner, using her scientific intuition to guide the simulation via a mouse or haptic device. This method has already been used in biomolecular research, for instance, to study the selectivity and regulation of the membrane channel protein GlpF and the enzyme glycerol kinase.[53] Setting up an IMD simulation is a straight-forward process that can be done on any computer.

The IMD haptic interface[52] consists of three primary components: a haptic device to provide translational and orientational input as well as force feedback to the user's hand; NAMD to calculate the effect of applied forces via molecular dynamics; and VMD to display results (Fig. 7). VMD communicates with the haptic device via a server[87] that controls the haptic environment experienced by the user, as described in ref. 52. The scheme of splitting the haptic, visualization, and simulation components into three communicating, asynchronous processes has been employed successfully,[52,88] and permits all three components to run at top speed, maximizing the responsiveness of the system. IMD requires

Figure 7. In IMD, the user applies forces to atoms in the simulation via a force-feedback haptic device.

efficient network communication between the visualization front-end and the MD back-end. Although the network bandwidth requirements for performing IMD are quite low relative to the computational demands, latency is a major concern as it has a direct impact on the responsiveness of the system. IMD uses custom networking code in NAMD and VMD to transfer atomic coordinates and steering forces efficiently.

To make molecular motion as described by MD perceptible to the IMD user through the haptic device, the quantities arising in the generic equation of motion governing the molecular response (represented below by Roman characters) and the haptic response (denoted by Greek characters),

$$m \frac{d^2x}{dt^2} = f, \quad \mu \frac{d^2\chi}{d\tau^2} = \phi \tag{20}$$

must be related through suitable scaling factors. Molecular motion probed is typically extended over distances of $x = 1$ Å, molecular time scales covered are typically $t = 1$ ps, and external forces acting on molecular moieties should not exceed $f = 1$ nN so as not to overwhelm inherent molecular forces. By contrast, the haptic device is characterized by length resolution of $\chi = 1$ cm and can generate a force of $\phi = 1$ N or more; $t = 1$ ps of dynamics requires $\tau = 1$ s or more to compute. The interface between the haptic device and NAMD thus introduces the scaling factors

$$S_x = \chi/x = 10^8, \quad S_t = \tau/t = 10^{12}, \quad S_f = \phi/f = 10^9, \tag{21}$$

Multiplying the molecular equation of motion in eq. (20) by the factor $S_f S_x / S_t^2$ gives

$$\frac{S_f S_x}{S_t^2} m \frac{d^2x}{dt^2} = S_f m \frac{d^2\chi}{d\tau^2} = \frac{S_f S_x}{S_t^2} f = \frac{S_x}{S_t^2} \phi. \tag{22}$$

From this we can conclude

$$\frac{S_f S_t^2}{S_x} m \frac{d^2\chi}{d\tau^2} = \phi. \tag{23}$$

Comparison with the haptic equation of motion in eq. (20) suggests that the effective mass felt by the haptic device, and hence, by the user is

$$\mu = \frac{S_f S_t^2}{S_x} m. \tag{24}$$

The molecular moieties to be moved through external forces have typical masses of (e.g., for glycerol moved through a membrane channel[53]) of $m = 180$ amu or $m \approx 3 \times 10^{-25}$ kg. From eq. (21) we conclude then that the effective mass felt by the user through the haptic device is 3 kg; the user does not sense strong inertial effects, and can readily manipulate the biomolecular system. IMD can also be carried out without force feedback, using a standard mouse to steer the simulated system.

To assist users of NAMD with IMD, AutoIMD[89] has been developed. AutoIMD permits the researcher to use the graphical interface provided by VMD to run an MD simulation based on a selection of atoms. The simulation can then be visualized in real time in the VMD graphics window. Forces may be applied with either a mouse or a haptic device by the user (as described above), or statically as in traditional SMD. Rather than carrying out a simulation of the entire molecule, AutoIMD performs a rapid MD simulation by dividing the system into three parts: a "molten zone," where the atoms are allowed to move freely; a surrounding "fixed zone," in which the atoms are included in the simulation (and exert forces on the molten zone), but are held fixed; and an "excluded zone," which is entirely disregarded in the AutoIMD simulation. In this way, AutoIMD may be used to inspect and perform energy minimizations on parts of the system that have been manipulated (e.g., through mutations or IMD), giving the researcher real-time feedback on the simulation.

SMD and IMD simulations differ in fundamental ways, and may be fruitfully combined. In SMD, the specification of the external forces is developed based on the researcher's understanding of the biological and structural properties of the system. The SMD simulation is carried out with the weakest force possible to induce the necessary change in an affordable length of simulation time, and the analysis of the simulation data relates the force applied to the progress of the system along the chosen reaction path. In contrast, IMD simulations are unplanned, allowing the researcher to toy with the system, exploring the degrees of freedom. Because the simulations need to be rapid—completed in minutes rather than days or weeks—the applied forces are extremely large, and the simulations are too rough to produce data suitable for an accurate analysis of molecular properties. The techniques can be combined: in the first stage, the researcher uses IMD to generate and test hypotheses for reaction mechanisms or to accelerate substrate transport, docking, and other mechanisms that are difficult to cast into numerical descriptions; in the second stage, the researcher carries out further MD or SMD simulations building on the hypothesized mechanisms or configurations from the IMD investigation.

Free Energy Calculations

In addition to propagating the motion of atoms in time, MD can also be used to generate an ensemble of configurations, from which thermodynamic quantities like free energy differences, ΔF, can be computed. In a nutshell, there are three possible routes for the calculation of ΔF: (1) estimate the relevant probability distribution, $\rho[U(\vec{r}_1, \ldots, \vec{r}_N)]$, from which a free energy difference may be inferred via $-1/\beta \ln \rho[U(\vec{r}_1, \ldots, \vec{r}_N)]/\rho_0$, where ρ_0 denotes a normalization term: (2) compute the free energy difference directly; and (3) calculate the free energy derivative, $d\Delta F(\xi)/d\xi$, along some order parameter (collective coordinate), ξ, consistent with an average force,[90] and integrate the latter to obtain ΔF.

The popular umbrella sampling method,[71,72] whereby the probability to find the system along a given reaction coordinate is sought, falls evidently into the first category. One blatant shortcoming of this scheme, however, lies in the need to guess the external potential or bias that is necessary to overcome the barriers of the free energy landscape—an issue that may rapidly become intricate in the case of qualitatively new problems. In this section,

we shall focus on the second and the third classes of approaches for determining free energy differences.

The first approach, available in NAMD since version 2.4, is free energy perturbation (FEP),[91] an exact method for the direct computation of relative free energies. FEP offers a convenient framework for performing "alchemical transformations," or *in silico* site-directed mutagenesis of one chemical species into another.

Description of intermolecular association or intramolecular deformation in complex molecular assemblies requires an efficient computational tool, capable of rapidly providing precise free energy profiles along some ordering parameter, ξ, in particular when little is known about the underlying free energy behavior of the process. A fast and accurate scheme, pertaining to the third category of methods, is introduced in NAMD version 2.6 to determine such free energy profiles, $\Delta F(\xi)$. This scheme relies upon the evaluation of the average force acting along the chosen order parameter, ξ, in such a way that no apparent free energy barrier impedes the progress of the system along the latter.[92,93]

The efficiency of the free energy algorithm represents only one facet of the overall performance of the free energy calculation, which to a large extent, relies on the ability of the core MD program to supply configurations and forces in rigorous thermodynamic ensembles and in a time-bound fashion. The methodology described hereafter has been implemented in NAMD and operates with nearly no extra cost compared to a standard MD simulation.

Alchemical Transformations

Contrary to the worthless piece of lead in the hands of the proverbial alchemist, the potential energy function of the computational chemist is sufficiently malleable to be altered seamlessly, thereby allowing the thermodynamic properties of a system to be related to those of a slightly modified one, such as a chemically modified protein or ligand, through the difference in the corresponding intermolecular potentials.

The free energy difference between a reference state, a, and a target state, b, can be expressed in terms of the ratio of their corresponding partition functions. Using the well-known relationship between partition function Z and free energy F, $Z = \exp[-F/k_BT]$, along with the property $Z = Z_{kin}Z_{pot}$ where Z_{kin} and Z_{pot} are the partition functions for kinetic and potential energy, respectively, one can express $F\Delta_{a \to b} = F_b - F_a$ as:

$$\Delta F_{a \to b} = -\frac{1}{\beta} \ln \frac{\int \exp[-\beta U_b(\vec{r}_1, \ldots, \vec{r}_N)]d\vec{r}_1 \ldots d\vec{r}_N}{\int \exp[-\beta U_a(\vec{r}_1, \ldots, \vec{r}_N)]d\vec{r}_1 \ldots d\vec{r}_N}. \quad (25)$$

Here U_a and U_b are the potential energy functions for states a and b, respectively. One can write eq. (25) $\Delta F_{a \to b} = -(1/\beta) \ln\{\int \exp[-\beta(U_b(\chi) - U_a(\chi))] \exp[-\beta U_a(\chi)]dx / \int \exp[-\beta U_a(\chi)]dx\}$ where $\chi = \vec{r}_1, \ldots, \vec{r}_N$. Defining the average, Boltzmann-weighted relative to the potential U_a, that is, weighted over configurations representative of the reference state a, $\langle f \rangle_a = \int f(\chi) \exp[-\beta U_a(\chi)]dx / \int \exp[-\beta U_a(\chi)]dx$, one can state:

$$\Delta F_{a \to b} = -\frac{1}{\beta} \ln \langle \exp\{-\beta[U_b(\vec{r}_1, \ldots, \vec{r}_N) - U_a(\vec{r}_1, \ldots, \vec{r}_N)]\}\rangle_a. \quad (26)$$

This is the celebrated FEP equation.[91] In principle, eq. (26) is *exact* in the limit of infinite sampling. In practice, however, on the basis of finite-length simulations, it only provides accurate estimates for small changes between a and b. This condition does not imply that the free energies characteristic of a and b be sufficiently close, but rather that the corresponding configurational ensembles overlap to a large degree to guarantee the desired accuracy. For example, although the hydration free energy of benzene is only -0.4 kcal/mol, insertion of a benzene molecule in bulk water constitutes too large a perturbation to fulfill the latter requirement in a single-step transformation. If such is not the case, the pathway connecting state a to state b is broken down into N intermediate, not necessarily physical states, λ_k ($a \equiv \lambda_1 = 0$ and $b \equiv \lambda_N = 1$), so that the Helmholtz free energy difference reads:

$$\Delta F_{a \to b} = -\frac{1}{\beta} \sum_{k=1}^{N-1} \ln\langle \exp\{-\beta[U(\vec{r}_1, \ldots, \vec{r}_N; \lambda_{k+1})$$
$$- U(\vec{r}_1, \ldots, \vec{r}_N; \lambda_k)]\}\rangle_{\lambda_k}. \quad (27)$$

Here the potential energy is not only a function of the spatial coordinates, but also of the parameter λ that connects the reference and the target states. Perturbation of the chemical system by means of λ_k may be achieved by scaling the relevant nonbonded force field parameters of appearing, vanishing, or changing atoms, in the spirit of turning lead into gold.

In NAMD, the topologies characteristic of the initial state, a, and the final state, b, coexist, yet without interacting. This implies that, as a preamble to the free energy calculation, a hybrid topology has to be defined with an appropriate exclusion list to prevent interactions between those atoms unique to state a and those unique to state b. In lieu of altering the nonbonded parameters, the interaction of the perturbed molecular fragments with their environment is scaled as a function of λ_k:

$$U(\vec{r}_1, \ldots, \vec{r}_N; \lambda_k) = \lambda_k U_b(\vec{r}_1, \ldots, \vec{r}_N)$$
$$+ (1 - \lambda_k) U_a(\vec{r}_1, \ldots, \vec{r}_N). \quad (28)$$

This scheme is referred to as the dual-topology paradigm.[94]

In a number of MD programs, FEP is implemented as an extra layer, implying that free energy differences are computed *a posteriori* by looping over a previously generated trajectory. In NAMD, the potential energies representative of the reference state, λ_k, and the target state, λ_{k+1}, are evaluated concurrently "on the fly" at little additional cost and the ensemble average of eq. (27) is updated continuously.

"Alchemical transformations" may be applied to a variety of chemically and biologically relevant systems, offering, in addition to a free energy difference, atomic-level insight into the structural modifications entailed by the perturbation. In Figure 8, *in silico* site-directed mutagenesis experiments are proposed for the transmembrane domain of glycophorin A (GpA) in an attempt to pinpoint those residues responsible for α-helix dimerization. Leu[75] and Ile[76] are perturbed into alanine following the depicted thermodynamic cycle. The first point mutation, L75A, yields a free energy change of $+13.9 \pm 0.3$ and $+28.8 \pm$
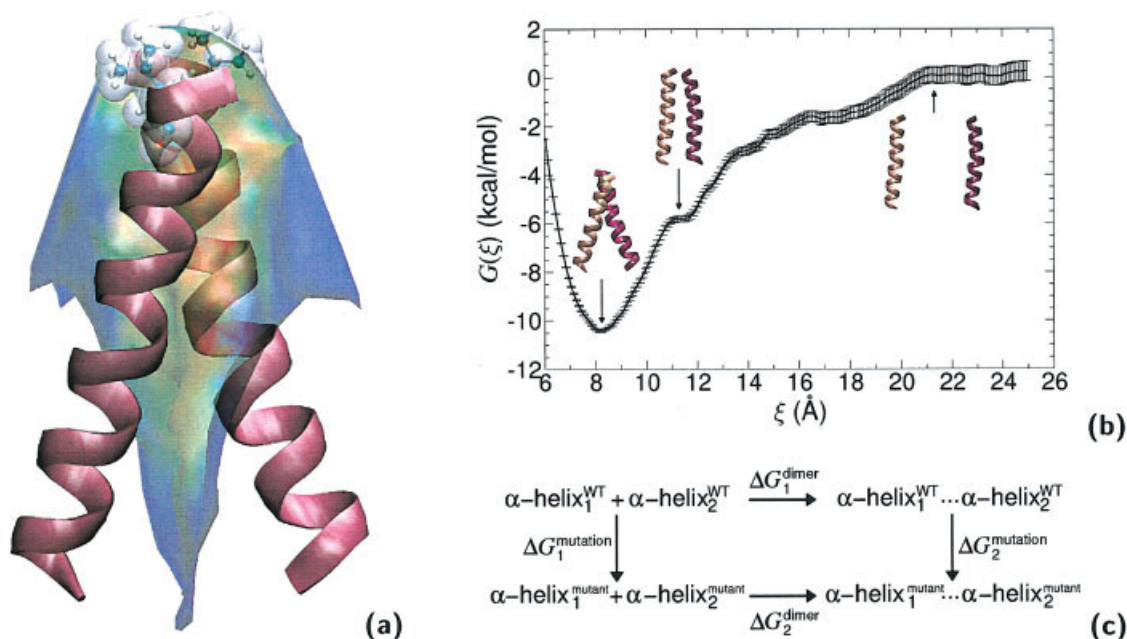
Figure 8. Homodimerization of the transmembrane (TM) domain of glycophorin A (GpA): (a) Contact surface of the two α-helices forming the TM domain of GpA. The strongest contacts are observed in the heptad of amino acids, Leu[75], Ile[76], Gly[79], Val[80], Gly[83], Val[84], and Thr[87]. Residue Leu[75], which participates in the association of the two α-helices through dispersive interactions, is featured as transparent van der Waals spheres. (b) Free energy profile delineating the reversible dissociation of the two α-helices, obtained using an adaptive biasing force. The ordering parameter, ξ, corresponds to the distance separating the center of mass of the TM segments. The entire pathway was broken down into 10 windows, in which up to 15 ns of MD sampling was performed, corresponding to a total simulation time of 125 ns. (c) Thermodynamic cycle utilized to perform the "alchemical transformation" of residues Leu[75] and Ile[76] into alanine, demonstrating the participation of these amino acids in the homodimerization of the two α-helices. The left vertical leg of the cycle represents the transformation in a single α-helix from the wild-type (WT) to the mutant form. The right vertical leg denotes a simultaneous point mutation in the two interacting α-helices. Using the notation of the figure, the free energy difference arising from this perturbation is equal to $\Delta G_2^{\text{mutation}} - 2\Delta G_1^{\text{mutation}}$. Each leg of the thermodynamic cycle consists of 50 intermediate states and a total MD sampling of 6 ns. For clarity, the environment of the α-helical dimer, formed by a dodecane slab in equilibrium between two lamellae of water, is not shown. [Color figure can be viewed in the online issue, which is available at www.interscience.wiley.com.]

0.5 kcal/mol in the free and in the bound state, respectively, which, put together, corresponds to a net free energy change of $+1.0 \pm 0.6$ kcal/mol (experimental estimate:[95] $+1.1 \pm 0.1$ kcal/mol). The second point mutation, I76A, led to a free energy change of -4.9 ± 0.3 and -8.4 ± 0.4 kcal/mol, in the single helix and in the dimer, respectively, that is, a net change of $+1.4 \pm 0.5$ kcal/mol (experimental estimate:[95] $+1.7 \pm 0.1$ kcal/mol). Aside from the remarkable agreement between theory and experiment, these free energy calculations confirm that replacement of bulky nonpolar side chains like leucine or isoleucine by alanine disrupts the α-helical dimer through a loss of van der Waals interactions.[96]

Overcoming Free Energy Barriers Using an Adaptive Biasing Force

The sizeable number of degrees of freedom described explicitly in statistical simulations of large molecular assemblies, in particular those of both chemical and biological interest, rationalizes the need

for a compact description of thermodynamic properties. Free energy profiles offer a suitable framework that fulfills this requirement by providing the dependence of the free energy on the chosen degrees of freedom ξ. Determination of such free energy profiles, under the *sine qua non* condition that some key degree of freedom ξ, for example, a reaction coordinate, can be defined, however, remains a daunting task from the perspective of numerical simulations. In the context of Boltzmann sampling of the phase space, overcoming the high free energy barriers that separate thermodynamic states of interest is a rare event that is unlikely to occur on the time scales amenable to MD simulation.

An important step forward on the road towards an optimal sampling of the phase space along a chosen collective coordinate, ξ, has been made recently. In a nutshell, this new method relies on the continuous application of a dynamically adapted biasing force that compensates the current estimate of the free energy, thus virtually erasing the roughness of the free energy landscape as the system progresses along ξ.[92] To reach this goal, the average force

acting on ξ, $\langle F_\xi \rangle_\xi$, is evaluated from an unconstrained MD simulation:[93]

$$\frac{dA(\xi)}{d\xi} = \left\langle \frac{\partial U(\vec{r}_1, \ldots, \vec{r}_N)}{\partial \xi} - \frac{1}{\beta} \frac{\partial \ln|J|}{\partial \xi} \right\rangle_\xi = -\langle F_\xi \rangle_\xi, \quad (29)$$

where $|J|$ denotes the determinant of the Jacobian for the transformation from Cartesian to generalized coordinates, which is a necessary modification of metric, given that $\{\vec{r}_1, \ldots, \vec{r}_N\}$ and ξ are not independent variables. The specific form of $|J|$ is an inherent function of the coordinate, ξ, chosen to advance the system.

In the course of the simulation in NAMD, the force, F_ξ, acting along the ordering parameter, ξ, is accrued in small bins, thereby supplying an estimate of the derivative $dA(\xi)/d\xi$. The so called adaptive biasing force (ABF), $\vec{F}^{ABF} = -\langle F_\xi \rangle_\xi \vec{\nabla}_r \xi$, is determined in such a way that, when applied to the system, it yields a Hamiltonian in which no average force is exerted along ξ. As a result, all values of ξ are sampled with an equal probability, which in turn, dramatically improves the accuracy of the calculated free energies. The approach further entails that progression of the system along ξ is fully reversible and limited solely by its self-diffusion properties. At this stage, it should be clearly understood that whereas the ABF method enhances sampling along ξ, its ability to supply a perfectly uniform probability distribution of the system over the entire range of ξ values may be impeded by possible orthogonal degrees of freedom.

We have chosen to introduce the average force method in NAMD within the convenient framework of *unconstrained* MD,[93] in which the coordinate, ξ is unconstrained, but other degrees of freedom, such as bond lengths, can be constrained. Either constraint forces must be taken into account in F_ξ, as they are in NAMD version 2.6, or it will be crucial to ascertain that no Cartesian coordinate appears simultaneously in a constrained degree of freedom and in the derivative $\partial U(\vec{r}_1, \ldots, \vec{r}_N)/\partial \xi$ of eq. (29).

The implementation of the ABF scheme in NAMD provides reaction coordinates such as a distance between subgroups of atoms or length along a specified direction in cartesian space. Previous applications include, the intramolecular folding of a short peptide, the partitioning of small solutes across an aqueous interface, and the intermolecular association of neutral and ionic species.[92,93]

The α-helical dimerization of GpA represents an interesting application of the method, whereby the reversible dissociation—rather than the association, for obvious cost-effectiveness reasons—is carried out, using the distance separating the center of mass of the trans-membrane segments as the reaction coordinate. The free energy profile characterizing this process is shown in Figure 8, and features a deep minimum at 8.2 Å, which corresponds to the native, close packing of the α-helices.

As the trans-membrane segments move away from each other, helix–helix interactions are progressively disrupted, in particular in the crossing region, thus causing an abrupt increase of the free energy, accompanied by a tilt of the two α-helices towards an upright orientation. As the distance between the two trans-membrane segments further increases, the free energy profile levels off at 21 Å, a separation beyond which the dimer is fully dissociated.

A valuable feature offered by NAMD lies in the possibility to evaluate *a posteriori* electrostatic and van der Waals forces from an ensemble of configurations. Projection of these forces onto the coordinate ξ, and subsequent integration of the former provides a deconvolution of the complete free energy profile in terms of helix–helix and helix–solvent contributions.

Analysis of these contributions reveals two regimes in the association process, driven at large separation by the solvent, which pushes the α-helices together, and at short separation by van der Waals interactions that favor native contacts.[96]

NAMD Software Design

Just as the intelligent car buyer looks under the hood to understand the performance and longevity of a particular vehicle, we now direct the attention of the reader and potential NAMD user to a few design and implementation details that contribute to the flexibility and performance of NAMD.

Goals, Design, and Implementation

NAMD was developed to enable ambitious MD simulations of biomolecular systems, employing the best technology available to provide the maximum performance possible to researchers. In the past decade simulation size and duration have increased dramatically. Ten years ago a simulation of 36,000 atoms over 100 ps as reported in ref. 5 was considered very advanced. Today, this status is reserved for simulations of systems with more than 300,000 atoms for up to 100 ns as reported in refs. 6, 23, and 55. The progress made is illustrated in Figure 1, comparing the sizes of systems reported in refs. 5 and 6. This 1000-fold increase in capability (10-fold in atom count and over 100-fold in simulation length) has been partially enabled by advances in processor performance, with clock rate increases leading the way. However, substantial progress has also resulted from exploiting the factor of 100 or more in performance available through the use of massively parallel computing, coordinating the efforts of numerous processors to address a single computation.

Looking forward, scientific ambition remains unchecked while increases in processor clock rates are constrained by limits on power consumption and heat dissipation. This stagnation in CPU speed has inspired system vendors such as Cray and SGI to incorporate field-programmable gate arrays (FPGAs) into their offerings, promising great performance increases, but only for suitable algorithms that are subjected to heroic porting efforts (as have been initiated for the force evaluations used by NAMD). Advances in semiconductor technology will surpass the limits encountered today, but in the meantime, industry has turned to offering greater concurrency to performance-hungry applications, scaling systems to more processors, and processors to more cores, rather than to higher clock rates. Indeed, the highest-performance component of a modern desktop is often the 3D graphics accelerator, which inexpensively provides an order of magnitude greater floating point capability than the main processor at a fraction of the clock rate by automatically distributing independent calculations to tens of pipelines, and even across multiple boards. Therefore, high performance and parallel computing will become even more synonymous than today, with greater industry acceptance and support.

Scientific computing is also facing the perennial "software crisis" that has stalked business information systems for decades. The seminal book by Allen and Tildesley[97] could dedicate a few pages of an appendix to writing efficient FORTRAN-77 code and consider the reader adequately informed. Developing modern high-performance software, however, requires knowledge of everything from parallel decomposition and coordination libraries to the relative cost of accessing different levels of cache memory. The design of more complex algorithms and numerical methods has ensured that any useful and successful program is likely to outlive the machine for which it is originally written, making portability a necessity. Software is also likely to be used and extended by persons other than the original author, making code readability and modifiability vital.

Software maintenance activities such as porting and modification account for the majority of the cost and effort associated with a program during its lifetime. These issues have been addressed in the development of object-oriented software design, in which the programmer breaks the program into "objects" comprising closely-related data (such as the x, y, and z components of a vector) and the operations that act on it (addition, dot product, cross product, etc.). The objects may be arranged into hierarchies of classes, and an object may contain or refer to other objects of the same or different classes. In this manner, large and complex programs can be broken down into smaller components with defined interfaces that can be implemented independently. NAMD is implemented in C++, the most popular and widely supported programming language providing efficient support for these methods.

Methodology for the development of parallel programs is far from mature, with automatically parallelizing compilers and languages still quite limited and most programmers using the Message Passing Interface (MPI) libraries in combination with C, C++, or Fortran. Although the acceptance of MPI as a crossplatform standard for parallel software has been of great benefit, the burden on the programmer remains. The first task is to decompose the problem, which is often simplified by assuming that the processor count is a power of two or has factors corresponding to the dimensions of a large three-dimensional array. MPI programming then requires the explicit sending and receiving of arrays between processors, much like directing a large and complex game of catch.

NAMD is based on the Charm++ parallel programming system and runtime library.[98] In Charm++, the computation is decomposed into objects that interact by sending messages to other objects on either the same or remote processors. These messages are asynchronous and one sided, that is, a particular method is invoked on an object whenever a message arrives for it rather than having the object waste resources while waiting for incoming data. This *message-driven object* programming style effectively hides communication latency and is naturally tolerant of the system noise that is found on workstation clusters. Charm++ also supports *processor virtualization*,[99] allowing each algorithm to be written for an ideal, maximum number of parallel objects that are then dynamically distributed among the actual number of processors on which the program is run. Charm++ provides these benefits even when it is implemented on top of MPI, an option that allows NAMD to be easily ported to new platforms.

The parallel decomposition strategy used by NAMD is to treat the simulation cell (the volume of space containing the atoms) as a three-dimensional patchwork quilt, with each *patch* of sufficient size that only the 26 nearest-neighboring patches are involved in bonded, van der Waals, and short-range electrostatic interactions. More precisely, the patches fill the simulation space in a regular grid and atoms in any pair of non-neighboring patches are separated by at least the cutoff distance at all times during the simulation. Each hydrogen atom is stored on the same patch as the atom to which it is bonded, and atoms are reassigned to patches at regular intervals. The number of patches varies from one to several hundred and is determined by the size of the simulation independently of the number of processors. Additional parallelism may be generated through options that double the number (and have the size) of patches in one or more dimensions.

When NAMD is run, patches are distributed as evenly as possible, keeping nearby patches on the same processor when there are more patches than processors, or spreading them across the machine when there are not. Then, a (roughly 14 times) larger number of *compute objects* responsible for calculating atomic interactions either within a single patch or between neighboring patches is distributed across the processors, minimizing communication by grouping compute objects responsible for the same patch together on the same processors. At the beginning of the simulation, the actual processor time consumed by each compute object is measured, and this data is used to redistribute compute objects to balance the workload between processors. This measurement-based load balancing[100] contributes greatly to the parallel efficiency of NAMD.

Using forces calculated by compute objects, each patch is responsible for integrating the equations of motion for the atoms it contains. This can be done independently of other patches, but occasionally requires global data affecting all atoms, such as a change in the size of the periodic cell due to a constant pressure algorithm. Although the integration algorithm is the clearly visible "outer loop" in a serial program, NAMD's message-driven design could have resulted in much obfuscation (as was experienced even in the simpler NAMD 1.X[4]). This was averted by using Charm++ threads to write a top-level function that is called once for each patch at program start and does not complete until the end of the simulation.[10] This design has allowed pressure and temperature control methods and even a conjugate gradient minimizer to be implemented in NAMD without writing any new code for parallel communication.

Tcl Scripting Interface

NAMD has been designed to be extensible by the end user in those areas that have required the most modification in the past and that are least likely to affect performance or harbor hard-to-detect programming errors. The critical force evaluation and integration routines that are the core of any molecular dynamics simulation have remained consistent in implementation as NAMD has evolved, occasionally introducing improved methods for pressure and temperature control. The greatest demand for modification has been in high-level protocols, such as equilibration and simulated annealing schedules. An additional demand has been for the implementation of experimental and often highly specialized steering and analysis methods, such as those used to study the rotational motion of ATP synthase.[85]

Flexibility requirements could, in theory, be met by having the end user modify NAMD's C++ source code, but this is undesirable for several reasons. Any users with special needs would have to maintain their own "hacked" version of the source code, which would need to be updated whenever a new version of NAMD was released. These unfortunate users would also need to maintain a full compiler environment and any external libraries for every platform on which they wanted to run NAMD. Finally, an understanding of both C++ and NAMD's internal structure would be required for any modification, and bugs introduced by the end user would be difficult for a novice programmer to fix. These problems can be eliminated by providing a scripting interface that is interpreted at run time by NAMD binaries that can be compiled once for each platform and installed centrally for all users on a machine.

Tcl (Tool Command Language)[102] is a popular interpreted language intended to provide a ready-made scripting interface to high-performance code written in a "systems programming language" such as C or C++. The Tcl programmer is supported by online documentation (at www.tcl.tk) and by books targeting all levels of experience. Tcl is used extensively in the popular molecular graphics program VMD, and therefore even novice users are likely to have experience with the language. In NAMD, Tcl is used to parse the simulation configuration file, allowing variables and expressions to be used in initially defining options, and then to change certain options during a running simulation.

Tcl scripting has been used to implement the replica exchange method[103] using NAMD, without modifying or adding a single line of C++. A master program, running in a Tcl shell outside of NAMD, is used to spawn a separate NAMD slave process for each replica needed. Each NAMD instance is started with a special configuration file that uses the standard networking capabilities of Tcl to connect to the master program via a TCP socket. At this point, the master program sends commands to each slave to load a molecule, simulate dynamics for a few hundred steps, report average energies, and change temperatures based on the relative temperatures of the other replicas. This work would have been much more difficult without a standard and fully featured scripting language such as Tcl.

NAMD provides a variety of standard steering forces and protocols, but an additional Tcl force interface provides the ultimate in flexibility. The user specifies the atoms to which steering forces will be applied; the coordinates of these atoms are then passed to a Tcl procedure, also provided by the user, at every time step. The Tcl steering procedure may use these atomic coordinates to calculate steering forces, possibly modifying them based on elapsed time or progress of the atoms along a chosen path. This minimal but complete interface has been used to implement complex features such as the adaptive biasing force method[93] described above.

Serial and Parallel Performance

Although the NAMD developers have strived to make the software as fast as possible,[104] decisions made by the user can greatly influence the serial performance and parallel efficiency of a particular simulation. For example, the computational effort required for a simulation is dominated by the nonbonded force evaluation, which scales as $NR_{\text{cut}}^3\rho$, where N is the number of simulated atoms,

R_{cut} is the cutoff distance, and $\rho = N/V$ is the number of atoms per unit volume. From this formula one can see that, for example, a five-point water model compared to a three-point water model increases both the number and density of simulated points (real and dummy atoms) and would therefore run up to $(5/3)^2 = 2.8$ times as long.

The processor type and clock rate of the machine on which NAMD is run, of course, will affect performance. Unlike many scientific codes, NAMD is usually limited by processor speed rather than memory size, bandwidth, or latency; the patch structure described above leads to naturally cache-friendly data layout and force routines. However, the nonbonded pair lists used by NAMD, while distributed across nodes in a parallel run, can result in paging to disk for large simulations on small memory machines, for example, 100,000 atoms on a single 128 MB workstation; in this case disabling pair lists will greatly improve performance.

The limits of NAMD's parallel scalability are mainly determined by atom count, with one processor per 1000 atoms being a conservative estimate for good efficiency on recent platforms. Increased cutoff distances will result in additional work to distribute, but also in fewer patches, and hence, one is confronted with a hard-to-predict effect on scaling. Finally, dynamics features that require global communication or even synchronization, such as minimization, constant pressure, or steering, may adversely affect parallel efficiency.

When procuring a parallel computer, great attention is normally paid to individual node performance, network bandwidth, and network latency. Although NAMD transfers relatively little data and is designed to be latency tolerant, scaling beyond a few tens of processors will benefit from the use of more expensive technologies than commodity gigabit ethernet. A major drain on parallel performance will come from interference by other processes running on the machine. A cluster should never be time shared, with two parallel jobs running on the same nodes at the same time, and care should be taken to ensure that orphaned processes from previous runs do not remain. On larger machines, even occasional interruptions for normal operating system functions have been shown to degrade the performance of tightly coordinated parallel applications running on hundreds of processors.[105]

The particle-mesh Ewald (PME) method for full electrostatics evaluation, neglected in the performance discussion thus far, deserves special attention. The most expensive parts of the PME calculation are the gridding of each atomic charge onto (typically) $4 \times 4 \times 4$ points of a regular mesh and the corresponding extraction of atomic forces from the grid; both scale linearly with atom count. The actual calculation of the (approximately) $100 \times 100 \times 100$ element fast Fourier transform (FFT) is negligible, but requires many messages for its parallel implementation. While this presents a serious impediment to other programs, NAMD's message-driven architecture is able to automatically interleave the latency-sensitive FFT algorithm with the dominant and latency-tolerant short-range nonbonded calculation.[106] In conclusion, a simulation with PME will run slightly slower than a non-PME simulation using the same cutoff, but PME is the clear winner because it provides physically correct electrostatics (without artifacts due to truncation) and allows a smaller short-range cutoff to be used.

When running on a parallel computer, it is important to measure the parallel efficiency of NAMD for the specific combination of hardware, molecular system, and algorithms of interest. This is correctly done by measuring the asymptotic cost of the simulation, that is, the additional runtime of a 2000 step run vs. a 1000 step run, thereby discounting startup and shutdown times. By measuring performance at a variety of processor counts, a decision can be made between, for example, running two jobs on 64 processors each vs. one job 60% faster (and 20% less efficiently) on 128 processors.

Dynamic load balancing makes NAMD's startup sequence longer than that of other parallel programs, requiring special attention to benchmarking. Initial load balancing in an NAMD run begins by default after five atom migration "cycles" of simulation. Compute object execution times are measured for five cycles, followed by a major load balancing in which work is reassigned to processors from scratch. Next is five cycles of measurement followed by a load balance refinement in which only minor changes are attempted. This is repeated immediately, and then periodically between 200-cycle stretches of simulation with measurement disabled (for maximum performance). After the second refinement, NAMD will print several explicitly labeled "benchmark" timings, which are a good estimate of performance for a long production simulation. The results of such benchmarking on a variety of platforms for a typical simulation are presented in Figure 9.

Although every researcher's situation is different, the computational resource decisions made by the authors' group provide a useful example. The main local resources are six independent, 24-node, 48-processor Linux clusters using commodity gigabit ethernet cards and switches. Each cluster is used for at most one simulation at a time, and therefore, only the six head nodes are connected to the building network, which provides access to central file and administrative servers. A queueing system manages a single queue, dispatching jobs to the next free cluster for up to 24 h, yielding full utilization as long as jobs are available to run. In addition, the Clustermatic Linux distribution allows a running simulation to be easily suspended by the queueing system, allowing short "express" jobs to run, which are used for simulation setup and testing, as well as for on-demand IMD. These cost-efficient local resources are supplemented by grants of computer time from NSF-funded centers, which provide access to larger, more scalable machines for large, intensive simulations and other special cases.

In conclusion, a basic understanding of NAMD's performance characteristics combined with specific benchmarks provides more science in less time. Conversely, the most common ways to waste computer time with NAMD are to include too much water in the simulation cell, to use an unnecessarily large cutoff with PME, to run on more processors than the simulation efficiency scales to, to blindly continue a simulation without checking the output for anomalies, and finally, to simulate a molecule without a clear understanding of what scientific questions are to be answered based on the results.

Three Exemplary Applications

In the following, we describe three exemplary applications of NAMD. The applications are chosen to illustrate the use of NAMD in studies of small (ubiquitin), intermediate (aquaporin channel), and large (*lac* repressor) systems. We emphasize in particular the features of NAMD that were most useful and how they allowed us to surmount methodological hurdles quickly.

Ubiquitin

One first application of the NAMD program involves a rather routine modeling project on a small protein system that grew into a more extensive one over time. The reader will learn from this first brief case study mainly how NAMD is used under common circumstances in which any other modeling program would have performed just as well, although we will emphasize the particular features that made NAMD a very suitable choice. The protein investigated is ubiquitin, which recently acquired considerable notice as the main subject of study by the 2004 Nobel laureates in Chemistry.[107,108] Ubiquitin is a small globular protein of about 80 amino acids that is highly conserved throughout the eukaryotes. The proteins, usually in the form of multimers, function as tags for the destination of cellular proteins in cell trafficking, for example, for protein degradation.[109] The modeling task in the present case was to explain atomic force microscopy experiments that measured forces and extensions that arise when monomeric or tetrameric ubiquitin is stretched with pN forces.[110,111] The project was vastly simplified through the availability of tutorials that explained how VMD and NAMD are used to set up a simulation of the solvated protein, to stretch it, and to analyze the results (http://www.ks.uiuc.edu/Training/Tutorials). Indeed, VMD and NAMD are accessible to novice researchers due to the extensive introductory material prepared by the developers.

The goal of these simulations was to stretch monomeric ubiquitin using the steered molecular dynamics method introduced above. After equilibration of the protein in a spherical water bath (a system of altogether 26,000 atoms) under NVT and NVE ensemble conditions with a 12 Å cutoff of nonbonded forces, the protein was stretched with the N-terminus constrained and the C-terminus pulled with a spring (spring constant of about 500 pN/Å), the end of which moved at a speed of 0.5 Å/ps [c.f., eq. (17) and Fig. 6]. Snapshots during the stretching process are shown in Figure 10. One can recognize that the protein can be stretched readily from the folded to the completely extended conformation. The simulations lasted about a nanosecond and, with a 2 fs time step, required 4 days on a desktop computer with an AMD Opteron processor.

Next, the stretching of a tandem of four ubiquitins was also attempted. In this case, the simulated protein-water system comprised 62,000 atoms; snapshots during the 3.5 ns stretching process are also shown in Figure 10. The simulations revealed the unfolding pathways of stretched ubiquitin, information that cannot be gleaned from an experiment that provides solely data of extension and applied forces vs. time. This application of steered molecular dynamics demonstrates well the value of molecular modeling in complementing experimental observation. The ready accessibility and ease of use of NAMD makes such modeling projects possible for experimentalists.

In this project several key features of NAMD and VMD were employed. NAMD ran on a common desktop system and was even used on a laptop, for example, for setting up and testing the
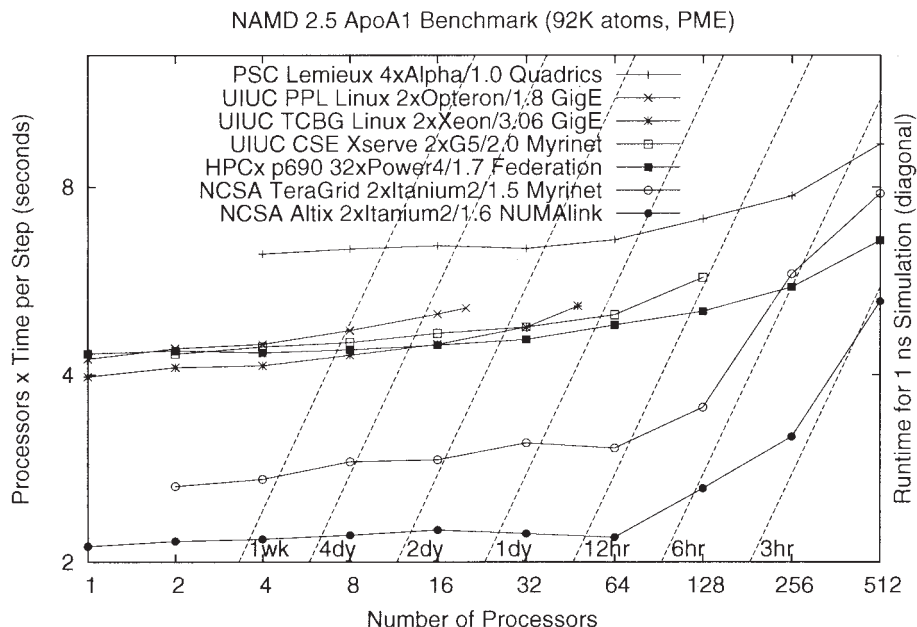
Figure 9. NAMD performance on modern platforms. The cost in CPU seconds of a single time step for a representative system of 92,000 atoms with a 12 Å short-range cutoff and full electrostatics evaluated via PME every four steps is plotted on the vertical axis, while the wait for a 1-ns simulation (one million time steps of 1 fs each) may be read relative to the broken diagonal lines. Perfect parallel scaling is a horizontal line. The older Pittsburgh Lemieux Alpha cluster has lower serial performance but scales very well. The HPCx IBM POWER 4 cluster at Edinburgh scales similarly, with comparable serial performance to the Xeon, Opteron, and Apple Xserve G5 clusters at UIUC. The two NCSA Itanium platforms have excellent serial performance but lose efficiency beyond 128 processors.

simulation. NAMD simulations can then easily be migrated to multiprocessor machines, although in the present case that was not absolutely necessary. The "Psfgen" plugin of VMD was very useful in setting up the system, namely in defining the chemical topology, that is, the LYS48-C-terminus bonds connecting the four tandem repeats, and generating so-called protein structure and parameter files. Also beneficial was the "Solvate" plugin of VMD, which greatly expedited the task of placing ubiquitin in a water bath. NAMD is ideally suited to carry out SMD simulations; as explained above, the needed functionality can be activated at the input file level and other features can be added through scripting. In the present case, the scripting capabilities of VMD allowed us to calculate the extension of the protein reached at any moment during the stretching process. This easy provision of all types of data from an MD run as well as the interplay with VMD are invaluable features of NAMD.

Aquaporin

The second example of using NAMD to simulate and investigate a biomolecular process concerns a family of membrane proteins, known as aquaporins (AQPs), which are responsible for facilitating water transfer across cellular membranes. Simulation of the dynamics and function of these channels is a good example of systems that require inclusion of more than 100,000 atoms in the molecular system,[112–115] as one needs to explicitly include a lipid bilayer and water to provide a natural environment to the protein and to be able to investigate transmembrane diffusion of molecules. Conceptual and methodological issues of simulating membrane proteins have been reviewed in refs. 116 and 117. The size of the system and the computational demand are usually prohibitive factors in simulation studies of membrane proteins, but NAMD's ability to exploit efficiently hundreds of processors makes it possible to tackle such problems with full atomic detail in the most faithful way possible. A side view of an AQP model embedded in a lipid bilayer is shown in Figure 11. AQPs are passive membrane channels that increase (over that of pure membranes) the rate of water exchange between the cell and its environment in a highly selective manner. Some members of the family have dual functions in cellular metabolism, as they also allow other small molecules, such as glycerol, to pass. Charged species, including protons, however, are excluded.

Simulation of water permeation through AQPs and the study of selectivity mechanisms employed by the channel require simulations of large molecular aggregates on the order of several tens of nanoseconds.[58,114,115,118] NAMD proved to be very efficient in simulating such systems at ambient pressure and physiological temperature with full account of electrostatic forces. These condi-
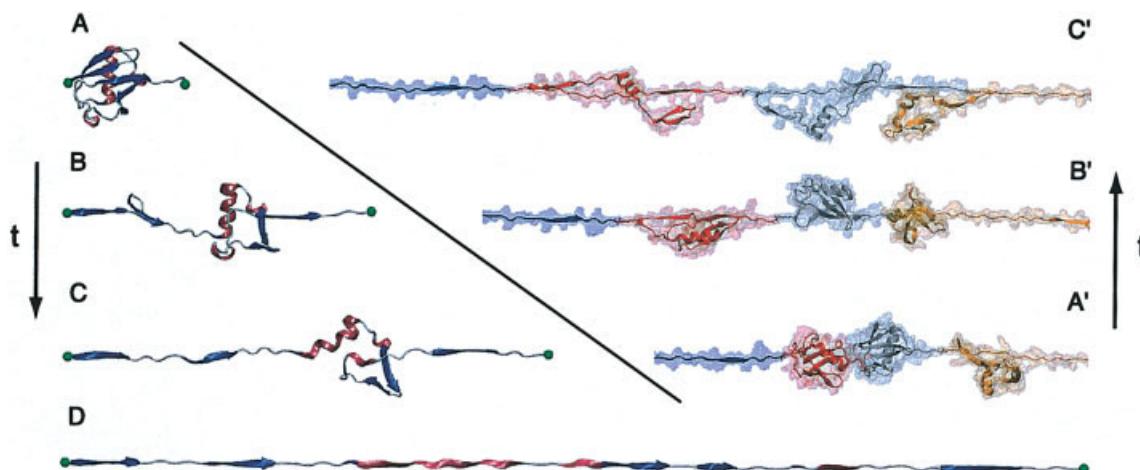
Figure 10. Pulling ubiquitin and tetra-ubiquitin. (A)–(D) mono-ubiquitin is shown at various stages of a constant velocity SMD simulation with the N- and C-termini highlighted in green. The different structures are seen to unfold at different moments in the simulation. (A′)–(C′) Tetra-ubiquitin is shown being pulled with constant force. Each color represents a different monomer and the transparent portion is the surface of the protein with the first and fourth segments not completely shown. Again, the different subunits can be seen to come apart at different times. [Color figure can be viewed in the online issue, which is available at www.interscience.wiley.com.]

tions are critical for a reliable description of the molecular system at hand. NAMD provides a variety of pressure control schemes that are effective and useful in the initial setup and equilibration phases of simulations. For example, NAMD allows exclusion of atoms from pressure calculation, which enables one to fix the protein during the initial simulation of its environment under constant-pressure conditions. Multi-nanosecond equilibrium simulations performed by NAMD successfully described diffusive permeation of water through the channel, in close agreement with the natural time scale (nanoseconds) of the event.[114,118] A key finding of the simulations was a unique configuration of water enforced by the channel during the permeation. This configuration was found to be an effective, novel selection mechanism that prevents proton transfer in these channels.[114,118] To investigate the permeation of larger substrates, that is, glycerol and longer linear sugar molecules, we took advantage of the SMD and IMD methodologies that are easily accessible through NAMD. SMD simulations of glycerol permeation through GlpF allowed us to reconstruct the potential of mean force of the process.[62] IMD simulations that permit one to rapidly sample various configurations of a complex between a macromolecule and small molecules were applied to study how sugar molecules interact with the narrowest part of the channel, the selectivity filter, and how these interactions furnish the stereoselectivity of the channel.[53]

The Tcl scripting capability of NAMD and its atom selection algorithms allowed us to apply external forces of different magnitude and direction to dynamically changing groups of water molecules, and thereby generate hydrostatic pressure gradients across the membrane.[58,115,119] Applying this method, and taking advantage of the speed of the simulations provided by NAMD and its high performance on various platforms (Fig. 9), we were able to calculate the water permeation rate through the channel using several simulations performed at various hydrostatic pressure gradients in either direction, and determine the osmotic permeability of AQPs, a property that can be directly compared to experimentally measured values for these channels.[58,115,119] In these simulations external forces were applied to a large group of molecules (water molecules in the bulk) whose number and positions are constantly changing as the simulations proceed. The modularity of the NAMD code allowed us to easily add the force application part of the calculations into the code, thus avoiding any compromise in the performance and scalability of the program. A very important advantage of NAMD in this respect is that the user does not need to know parallel programming to implement new features and add modules to the program.

Multiscale lac *Repressor–DNA Complex*

Our third example for the use of NAMD concerns a protein–DNA complex involving the *lac* repressor (LacI) that is a paradigm for gene control. We choose this example because it leads to a simulation of very large size (314,000 atoms) that also requires great flexibility in the simulation protocol in combining all-atom molecular dynamics with continuum mechanics.

LacI regulates the function of the *lac* operon, a set of genes responsible for lactose digestion in *Escherichia coli;* when lactose is not present as a metabolite in the environment, LacI inhibits the expression of these genes by binding to two nearby sites at the beginning of the operon and folding the intervening DNA into a loop. The detailed mechanics of the LacI–DNA interaction remain unknown even though the crystallographic structure of LacI bound to its cognate DNA segments is available[120,121] along with exten-
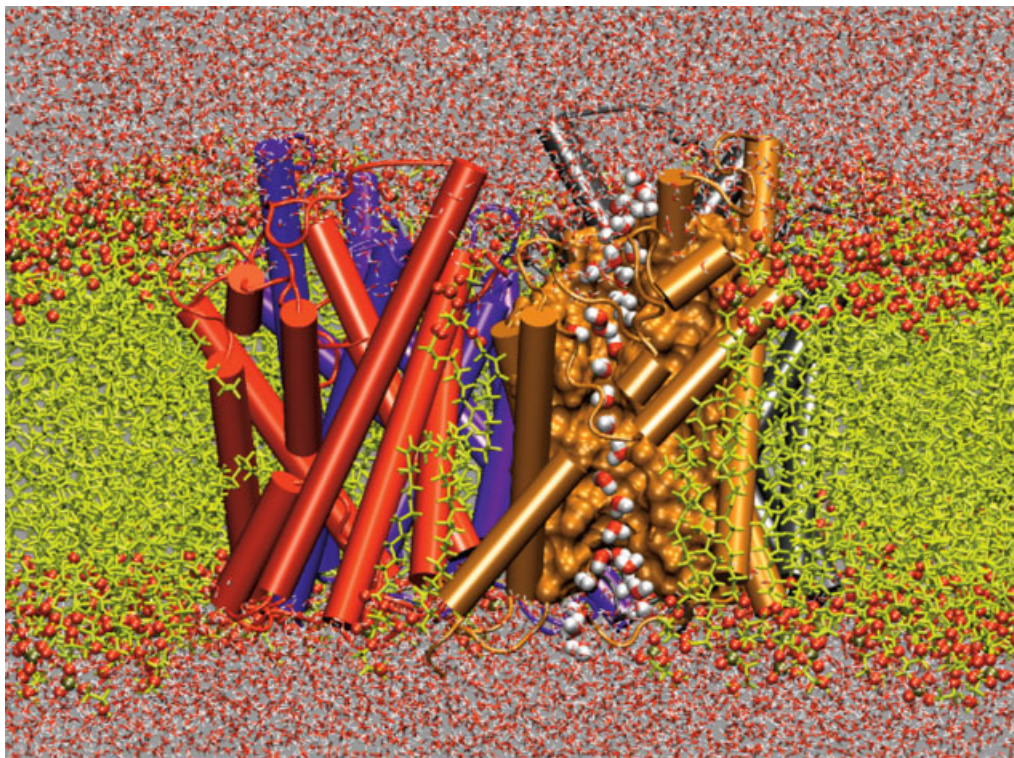
Figure 11. Side view of a simulated aquaporin tetramer in the cell membrane. The *E. coli* water/glycerol channel GlpF is embedded in a patch of POPE lipid bilayer and fully hydrated by water on both sides. Lipid head groups are shown in CPK and the hydrophobic tail region is drawn using licorice representation. The four AQP monomers, each forming an independent water pore, are shown in different colors. The single file of water formed inside the pores is shown in one of the monomers. The characteristic conformational inversion of water at the center of the channel that contributes to the barrier against proton transfer is discernible.

sive biochemical and genetic data.[122,123] In particular, the structure in ref. 120 does not include the DNA loop connecting the two bound DNA segments nor does it provide information on how LacI wrestles the DNA, forcing it to maintain a loop form.

A key obstacle to the simulation of the LacI–DNA dynamics is that LacI alone is a very large protein that results, together with a water bath, in a system of 300,000 atoms; including the DNA loop would increase the size to 700,000 atoms, thus incurring an even greater computational cost. To overcome this difficulty one can follow a multiscale strategy and describe the DNA loop mathematically employing the Kirchhoff theory of continuum elastic rods as developed in ref. 124, coupling the calculation to an all-atom MD representation of LacI. The method has been outlined in ref. 86 and applied in ref. 6. The LacI–DNA structure constructed in ref. 125 and employed in ref. 6 is available in the Protein Data Bank (1Z04).[126] In the simulation, illustrated in Figure 12, LacI was solvated in a box of TIP3P water and 100 mM NaCl and simulated under NPT ensemble conditions with periodic boundary conditions and PME electrostatics for an overall simulation time of 40 ns using a 1-fs time step. At 10-ps intervals, position and orientation of the LacI head groups were communicated to the mathematical description of the DNA loop, which

determined the appropriate new loop geometry and communicated back the forces and torques with which the DNA resisted the protein's action; forces and torques were included in the MD simulations much like forces are incorporated in SMD runs. Simulation results are shown in Figure 12. One can recognize the large scale motion of the DNA loop over the course of the simulation. A key finding resulting from the simulation is an extreme flexibility of the two LacI head groups absorbing most of the strain arising from the DNA loop. The simulations reported in ref. 6 also provided an insightful new interpretation of prior FRET data.[127]

NAMD proved to be most valuable due to its ability to efficiently simulate very large systems. In the present case NAMD ran a 314,000 atom system on 256 Itanium processors of the NCSA TeraGrid system with an average production speed of 2.5 ns per day. The multiscale strategy linking MD with a continuum mechanics DNA model was implemented through the Tcl scripting interface of NAMD. This feature permitted us not only to obtain information from the simulation, for example, head group geometries, on the fly, but also to control from the NAMD side the calculations for the DNA model, eventually retrieving the forces applied in the LacI simulation. For the sake of clarity we emphasize that the entire multiscale simulation, including the continuum
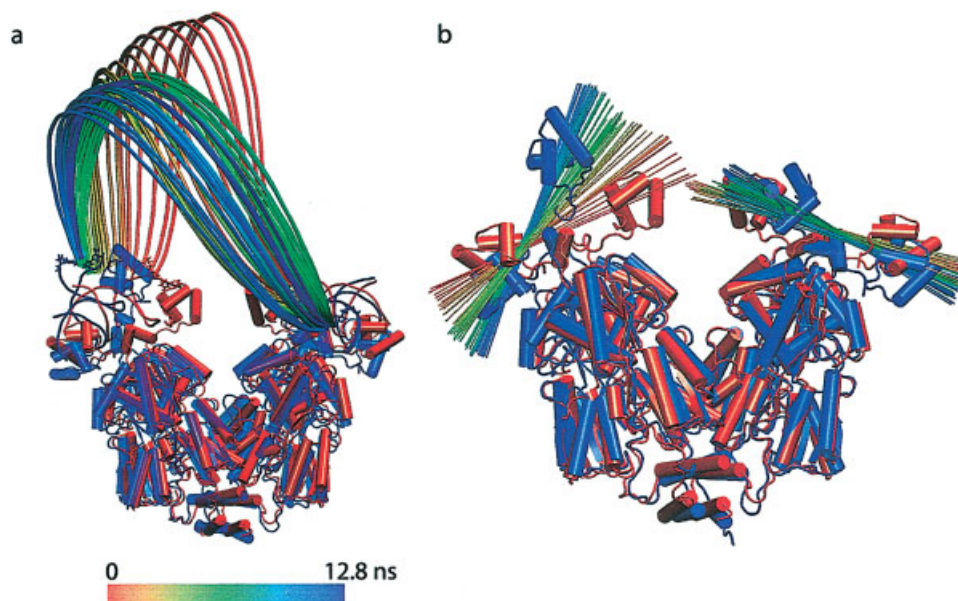
Figure 12. Snapshots taken over the course of the LacI–DNA complex multiscale simulation: (a) The evolution of the structure of the DNA loop; (b) The structure of LacI remains unchanged, with the exception of the rotation of the head groups, which allows the DNA loop to adopt a more relaxed configuration.

mechanics description of DNA, was controlled from the NAMD program and its Tcl scripting feature. Because NAMD readily permits the definition of all types of external forces, the implementation of the multiscale strategy was straightforward. We note here also that the ability of NAMD to write and read any type of files during its execution proved to be invaluable for the ultimate analysis of the multiscale simulation data.

Conclusion

We conclude our overview of NAMD with a list of the program's key features in Table 1. Surveys indicate consistently that users greatly appreciate that NAMD is distributed free of charge. NAMD is well known for its performance on large parallel computers, for which it has received a Gordon Bell award,[106] but the program is actually used on many platforms, including laptops. This versatility is a great benefit for initiating and testing modeling projects. NAMD permits a novice to carry out standard simulations of most types readily, but NAMD also supports more advanced uses. The most essential feature in this regard is NAMD's Tcl scripting capability, which has been used to implement, for example, replica exchange dynamics, adaptive biasing forces, and advanced phase space sampling protocols.

NAMD is complemented by the molecular graphics program VMD to offer a complete modeling environment. In addition to its other functions, VMD provides tools tailored to NAMD. This is a natural development because not only do the programs share a large common user base, but they are also being developed together and use the same scripting language. VMD provides assistance at all stages of a simulation including preparing the initial system, monitoring the progress of the calculation, and analyzing the results. Initiating a modeling project is simplified and accelerated through convenient features that aid in the typical tasks of building a model, for example, solvating a protein or placing it in a lipid bilayer, and providing the needed protein structure files. VMD's AutoIMD feature allows one to modify and/or interact with the system "on the fly" with both immediate visual and mechanical feedback, thus providing an intuitive method of exploring the system in ways not available through scripting alone. Finally, VMD provides a unique analysis environment for the results of NAMD simulations. For example, one can use VMD for routine calculations such as protein stability or intra- and intermolecular distances, as well as advanced ones such as electrostatic potential maps. Furthermore, the analysis capabilities of VMD may be extended through Tcl scripting, allowing the user to design any project-specific tools needed. Clearly, although NAMD and VMD function effectively as stand-alone programs, their highest purpose is achieved when used together.

NAMD users also benefit from the program BioCoRE,[128] a Web-based collaborative research environment that is linked to both NAMD and VMD. For example, BioCoRE greatly simplifies submission of NAMD simulations to supercomputer centers and local machines alike. BioCoRE also provides a graphical user interface to prepare simulation input files.

The authors' Urbana group focuses much effort on training researchers in the use of NAMD through a series of tutorials available on the Web. The NAMD Web site is a continuously updated source of information for novice and advanced users (http://www.ks.uiuc.edu/Research/namd/).

Table 1. Key Features of NAMD.

Ease of use

Free to download and use.

Precompiled binaries provided for 12 popular platforms.

Installed at major NSF supercomputer sites.

Portable to virtually any desktop, cluster, or other parallel computer.

C++ source code and CVS access for modification.

Molecule building

Reads X-PLOR, CHARMM, AMBER, and GROMACS input files.

Psfgen tool generates structures and coordinate files for CHARMM force field.

Efficient conjugate gradient minimization.

Fixed atoms and harmonic restraints.

Thermal equilibration via periodic rescaling, reinitialization, or Langevin dynamics.

Basic simulation

Constant temperature via rescaling, coupling, or Langevin dynamics.

Constant pressure via Berendsen or Langevin–Hoover methods.

Particle-mesh Ewald full electrostatics for periodic systems.

Symplectic multiple time step integration.

Rigid water molecules and bonds to hydrogen atoms.

Advanced simulation

Alchemical and conformational free energy calculations.

Automated pair-interaction calculations.

Automated pressure profile calculations.

Locally enhanced sampling via multiple images.

Tcl based scripting and steering forces.

Interactive visual steering interface to VMD.

Acknowledgments

References

1. Kalé, L.; Skeel, R.; Bhandarkar, M.; Brunner, R.; Gursoy, A.; Krawetz, N.; Phillips, J.; Shinozaki, A.; Varadarajan, K.; Schulten, K. J Comp Phys 1999, 151, 283.

2. Humphrey, W.; Dalke, A.; Schulten, K. J Mol Graphics 1996, 14, 33.

3. Nelson, M.; Humphrey, W.; Gursoy, A.; Dalke, A.; Kalé, L.; Skeel, R.; Schulten, K.; Kufrin, R. Comput Phys Commun 1995, 91, 111.

4. Nelson, M.; Humphrey, W.; Gursoy, A.; Dalke, A.; Kalé, L.; Skeel, R. D.; Schulten, K. Int J Supercomp Appl High Perform Comp 1996, 10, 251.

5. Kosztin, D.; Bishop, T. C.; Schulten, K. Biophys J 1997, 73, 557.

6. Villa, E.; Balaeff, A.; Schulten, K. Proc Natl Acad Sci USA 2005, 102, 6783.

7. MacKerell, A. D., Jr.; Bashford, D.; Bellott, M.; Dunbrack, R. L., Jr.; Evanseck, J.; Field, M. J.; Fischer, S.; Gao, J.; Guo, H.; Ha, S.; Joseph, D.; Kuchnir, L.; Kuczera, K.; Lau, F. T. K.; Mattos, C.; Michnick, S.; Ngo, T.; Nguyen, D. T.; Prodhom, B.; Reiher, I. W. E.; Roux, B.; Schlenkrich, M.; Smith, J.; Stote, R.; Straub, J.; Watanabe, M.; Wiorkiewicz–Kuczera, J.; Yin, D.; Karplus, M. J Phys Chem B 1998, 102, 3586.

8. Weiner, S. P.; Kollman, P. A.; Case, D. A.; Singh, U. C.; Ghio, C.; Alagona, G.; Profeta, J.; Weiner, P. J Am Chem Soc 1984, 106, 765.

9. Berendsen, H. J. C.; van der Spoel., D.; van Drunen, R. Comput Phys Commun 1995, 91, 43.

10. Weiner, P. K.; Kollman, P. A. J Comp Chem 1981, 2, 287.

11. Ewald, P. Ann Phys 1921, 64, 253.

12. de Leeuw, S. W.; Perram, J. W.; Smith, E. R. Proc R Soc Lond A 1980, 373, 27.

13. Grubmüller, H.; Heller, H.; Windemuth, A.; Schulten, K. Mol Simulat 1991, 6, 121.

14. Loncharich, R. J.; Brooks, B. R. Proteins Struct Funct Genet 1989, 6, 32.

15. Feller, S. E.; Pastor, R. W.; Rojnuckarin, A.; Bogusz, S.; Brooks, B. R. J Phys Chem 1996, 100, 17011.

16. Bergdorf, M.; Peter, C.; Hünenberger, P. H. J Chem Phys 2003, 119, 9129.

17. Kastenholz, M. A.; Hünenberger, P. H. J Phys Chem B 2004, 108, 774.

18. Weber, W.; Hünenberger, P. H.; McCammon, J. A. J Phys Chem B 2000, 104, 3668.

19. Perram, J. W.; Petersen, H. G.; de Leeuw, S. W. Mol Phys 1988, 65, 875.

20. Darden, T. A.; York, D. M.; Pedersen, L. G. J Chem Phys 1993, 98, 10089.

21. Essmann, U.; Perera, L.; Berkowitz, M. L.; Darden, T.; Lee, H.; Pederson, L. J Chem Phys 1995, 103, 8577.

22. Hairer, E.; Lubich, C.; Wanner, G. Geometric Numerical Integration, vol. 31 in Springer Series in Computational Mathematics; Springer-Verlag: Berlin, 2002.

23. Aksimentiev, A.; Schulten, K. Biophys J 2005, 88, 3745.

24. Hockney, R. W.; Eastwood, J. W. Computer Simulation Using Particles; McGraw-Hall: New York, 1981.

25. Skeel, R. D.; Tezcan, I.; Hardy, D. J. J Comput Chem 2002, 23, 673.

26. Brandt, A.; Lubrecht, A. A. J Comput Phys 1990, 90, 348.

27. Arnol'd, V. I. Mathematical Methods of Classical Mechanics; Springer-Verlag: New York, 1989, 2nd ed.

28. Reich, S. SIAM J Numer Anal 1999, 36, 1549.

29. Harvey, S. C. Proteins Struct Funct Genet 1989, 5, 78.

30. Dahlquist, G.; Björck, Å. Numerical Methods; Prentice Hall: Englewood Cliffs, NJ, 1974.

31. Frenkel, D.; Smit, B. Understanding Molecular Simulation from Algorithms to Applications; Academic Press: San Diego, CA, 2002.

32. Gear, C. W. Numerical Initial Value Problems in Ordinary Differential Equations; Prentice-Hall: Englewood Cliffs, NJ, 1971.

33. Tuckerman, M.; Berne, B. J.; Martyna, G. J. J Chem Phys 1992, 97, 1990.

34. Grubmüller, H. Master's thesis, Physik-Dept. der Tech. Univ., Munich, Germany, 1989.

35. Bishop, T. C.; Skeel, R. D.; Schulten, K. J Comp Chem 1997, 18, 1785.

36. Ma, Q.; Izaguirre, J. A.; Skeel, R. D. SIAM J Sci Comput 2003, 24, 1951.

37. Kubo, R.; Toda, M.; Hashitsume, N. Statistical Physics II: Nonequilibrium Statistical Mechanics; Springer: New York, 1991, 2nd ed.

38. Brünger, A.; Brooks, C. B.; Karplus, M. Chem Phys Lett 1984, 105, 495.

39. Mishra, B.; Schlick, T. J Chem Phys 1996, 105, 299.

40. Wang, W.; Skeel, R. D. Mol Phys 2003, 101, 2149.

41. Park, S.; Schulten, K. J Chem Phys 2004, 120, 5946.

42. Tuckerman, M.; Liu, Y.; Ciccotti, G.; Martyna, G. J. J Chem Phys 2001, 115, 1678.

43. Bhandarkar, M.; Brunner, R.; Chipot, C.; Dalke, A.; Dixit, S.; Grayson, P.; Gullingsrud, J.; Gursoy, A.; Hardy, D.; Humphrey, W.; Hurwitz, D.; Krawetz, N.; Nelson, M.; Phillips, J.; Shinozaki, A.; Zheng, G.; Zhu, F. NAMD user's guide version 2.5. http://www.ks.uiuc.edu/Research/namd/2.5/ug/ug.html.

44. Feller, S. E.; Zhang, Y.; Pastor, R. W.; Brooks, B. R. J Chem Phys 1995, 103, 4613.

45. Hoover, W. G. Phys Rev A 1985, 31, 1695.

46. Hoover, W. G. Phys Rev A 1986, 34, 2499.

47. Hoover, W. G. Computational Statistical Mechanics; Elsevier: Amsterdam, 1991.

48. Quigley, D.; Probert, M. I. J. J Chem Phys 2004, 120, 11432.

49. Izrailev, S.; Stepaniants, S.; Isralewitz, B.; Kosztin, D.; Lu, H.; Molnar, F.; Wriggers, W.; Schulten, K. Computational Molecular Dynamics: Challenges, Methods, Ideas, vol. 4 in Lecture Notes in Computational Science and Engineering; Deuflhard, P.; Hermans, J.; Leimkuhler, B.; Mark, A. E.; Reich, S.; Skeel, R. D., Eds.; Springer-Verlag: Berlin, 1998, p. 39.

50. Isralewitz, B.; Baudry, J.; Gullingsrud, J.; Kosztin, D.; Schulten, K. J Mol Graph Model 2001, 19, 13; Also in Protein Flexibility and Folding, Kuhn, L. A.; Thorpe, M. F., Eds.; Elsevier: New York.

51. Isralewitz, B.; Gao, M.; Schulten, K. Curr Opin Struct Biol 2001, 11, 224.

52. Stone, J.; Gullingsrud, J.; Grayson, P.; Schulten, K. In 2001 ACM Symposium on Interactive 3D Graphics; Hughes, J. F.; Séquin, C. H., Eds.; ACM SIGGRAPH: New York, 2001, p. 191.

53. Grayson, P.; Tajkhorshid, E.; Schulten, K. Biophys J 2003, 85, 36.

54. Gullingsrud, J.; Braun, R.; Schulten, K. J Comp Phys 1999, 151, 190.

55. Sotomayor, M.; Corey, D. P.; Schulten, K. Structure 2005, 13, 669.

56. Craig, D.; Gao, M.; Schulten, K.; Vogel, V. Structure 2004, 12, 2049.

57. Aksimentiev, A.; Balabin, I. A.; Fillingame, R. H.; Schulten, K. Biophys J 2004, 86, 1332.

58. Zhu, F.; Tajkhorshid, E.; Schulten, K. Biophys J 2004, 86, 50.

59. Gullingsrud, J.; Schulten, K. Biophys J 2003, 85, 2087.

60. Bayas, M. V.; Schulten, K.; Leckband, D. Biophys J 2003, 84, 2223.

61. Gao, M.; Wilmanns, M.; Schulten, K. Biophys J 2002, 83, 3435.

62. Jensen, M. Ø.; Park, S.; Tajkhorshid, E.; Schulten, K. Proc Natl Acad Sci USA 2002, 99, 6731.

63. Kosztin, D.; Izrailev, S.; Schulten, K. Biophys J 1999, 76, 188.

64. Lu, H.; Schulten, K. Proteins Struct Funct Genet 1999, 35, 453.

65. Stepaniants, S.; Izrailev, S.; Schulten, K. J Mol Mod 1997, 3, 473.

66. Izrailev, S.; Crofts, A. R.; Berry, E. A.; Schulten, K. Biophys J 1999, 77, 1753.

67. Izrailev, S.; Stepaniants, S.; Balsera, M.; Oono, Y.; Schulten, K. Biophys J 1997, 72, 1568.

68. Isralewitz, B.; Izrailev, S.; Schulten, K. Biophys J 1997, 73, 2972.

69. Grubmüller, H.; Heymann, B.; Tavan, P. Science 1996, 271, 997.

70. Kosztin, D.; Izrailev, S.; Schulten, K. Biophys J 1999, 76, 188.

71. Torrie, G. M.; Valleau, J. P. J Comput Phys 1977, 23, 187.

72. Roux, B. Comput Phys Commun 1995, 91, 275.

73. Schulten, K.; Schulten, Z.; Szabo, A. J Chem Phys 1981, 74, 4426.

74. Lu, H.; Krammer, A.; Isralewitz, B.; Vogel, V.; Schulten, K. In Elastic Filaments of the Cell; Pollack, J.; Granzier, H., Eds.; Kluwer Academic/Plenum Publishers: New York, 2000, p. 143, chap 1.

75. Lu, H.; Schulten, K. Biophys J 2000, 79, 51.

76. Jarzynski, C. Phys Rev Lett 1997, 78, 2690.

77. Jarzynski, C. Phys Rev E 1997, 56, 5018.

78. Liphardt, J.; Dumont, S.; Smith, S.; Tinoco, I.; Bustamante, C. Science 2002, 296, 1832.

79. Hummer, G.; Rasaiah, J. C.; Noworyta, J. P. Nature 2001, 414, 188.

80. Marcinkiewicz, J. Math Z 1939, 44, 612.

81. Park, S.; Khalili-Araghi, F.; Tajkhorshid, E.; Schulten, K. J Chem Phys 2003, 119, 3559.

82. Kumar, S.; Bouzida, D.; Swendsen, R. H.; Kollman, P. A.; Rosenberg, J. M. J Comp Chem 1992, 13, 1011.

83. Boczko, E. M.; Brooks, C. L., III. J Phys Chem 1993, 97, 4509.

84. Shea, J. E.; Brooks, C. L., III. Annu Rev Phys Chem 2001, 52, 499.

85. Aksimentiev, A.; Balabin, I. A.; Fillingame, R. H.; Schulten, K. Biophys J 2004, 86, 1332.

86. Villa, E.; Balaeff, A.; Mahadevan, L.; Schulten, K. Multiscale Model Simul 2004, 2, 527.

87. Taylor, R. M., II. VRPN: Virtual Reality Peripheral Network, 1998. http://www.cs.unc.edu/Research/vrpn.

88. Dachille, F.; Qin, H.; Kaufman, A.; El-Sana, J. In 1999 Symposium on Interactive 3D Graphics, 1999, p. 103.

89. Cohen, J.; Grayson, P. AutoIMD User's Guide, 2003. http://www.ks.uiuc.edu/Research/vmd/plugins/autoimd.

90. den Otter, W. K.; Briels, W. J. J Chem Phys 1998, 109, 4139.

91. Zwanzig, R. W. J Chem Phys 1954, 22, 1420.

92. Darve, E.; Pohorille, A. J Chem Phys 2001, 115, 9169.

93. Hénin, J.; Chipot, C. J Chem Phys 2004, 121, 2904.

94. Gao, J.; Kuczera, K.; Tidor, B.; Karplus, M. Science 1989, 244, 1069.

95. Fleming, K. G.; Ackerman, A. L.; Engelman, D. M. J Mol Biol 1997, 272, 266.

96. Hénin, J.; Pohorille, A.; Chipot, C. J Am Chem Soc 2005, 127, 8478.

97. Allen, M. P.; Tildesley, D. J. Computer Simulation of Liquids; Oxford University Press: New York, 1987.

98. Kalé, L. V.; Krishnan, S. Parallel Programming using C++; Wilson, G. V.; Lu, P., Eds.; MIT Press: Cambridge, MA, 1996, p. 175.

99. Kalé, L. V. In LACSI 2002; Albuquerque, 2002.

100. Brunner, R. K.; Kalé, L. V. In Parallel and Distributed Computing for Symbolic and Irregular Applications; World Scientific Publishing: Singapore, 2000, p. 167.

101. Phillips, J. C.; Brunner, R.; Shinozaki, A.; Bhandarkar, M.; Krawetz, N.; Kalé, L.; Skeel, R. D.; Schulten, K. In Computational Molecular Dynamics: Challenges, Methods, Ideas; vol. 4 in Lecture Notes in Computational Science and Engineering; Deuflhard, P.; Hermans, J.; Leimkuhler, B.; Mark, A.; Reich, S.; Skeel, R. D., Eds.; Springer-Verlag: Berlin, 1998, p. 472.

102. Ousterhout, J. Tcl and the Tk Toolkit; Addison-Wesley: Reading, MA; 1994.

103. Sugita, Y.; Okamoto, Y. Chem Phys Lett 1999, 314, 141.

104. Kale, L. V.; Zheng, G.; Lee, C. W.; Kumar, S. In Future Generation Computer Systems Special Issue on: Large-Scale System Performance Modeling and Analysis; in press.

105. Petrini, F.; Kerbyson, D. J.; Pakin, S. In Proceedings of the IEEE/ACM SC2003 Conference, Technical Paper 301; IEEE Press: Piscataway, NJ, 2003.

106. Phillips, J.; Zheng, G.; Kumar, S.; Kale, L. In Proceedings of the IEEE/ACM SC2002 Conference, Technical Paper 277; IEEE Press: Piscataway, NJ, 2002.

107. Hershko, A.; Heller, H.; Elias, S.; Ciechanover, A. J Biol Chem 1983, 258, 8206.

108. Haas, A. L.; Rose, I. A. J Biol Chem 1982, 257, 10329.

109. Hershko, A.; Ciechanover, A. Annu Rev Biochem 1998, 67, 425.

110. Carrion–Vazquez, M.; Li, H.; Lu, H.; Marszalek, P. E.; Oberhauser, A. F.; Fernandez, J. M. Nat Struct Biol 2003, 10, 738.

111. Fernandez, J. M.; Li, H. Science 2004, 303, 1674.

112. Zhu, F.; Tajkhorshid, E.; Schulten, K. FEBS Lett 2001, 504, 212.

113. Jensen, M. Ø; Tajkhorshid, E.; Schulten, K. Structure 2001, 9, 1083.

114. Tajkhorshid, E.; Nollert, P.; Jensen, M. Ø; Miercke, L. J. W.; O'Connell, J.; Stroud, R. M.; Schulten, K. Science 2002, 296, 525.

115. Zhu, F.; Tajkhorshid, E.; Schulten, K. Biophys J 2002, 83, 154.

116. Roux, B.; Schulten, K. Structure 2004, 12, 1343.

117. Tajkhorshid, E.; Cohen, J.; Aksimentiev, A.; Sotomayor, M.; Schulten, K. In Bacterial Ion Channels and Their Eukaryotic Homologues; Martinac, B.; Kubalski, A., Eds.; ASM Press: Washington, DC, 2005, p. 153.

118. Jensen, M. Ø; Tajkhorshid, E.; Schulten, K. Biophys J 2003, 85, 2884.

119. Zhu, F.; Tajkhorshid, E.; Schulten, K. Phys Rev Lett 2004, 93, 224501.

120. Lewis, M.; Chang, G.; Horton, N. C.; Kercher, M. A.; Pace, H. C.; Schumacher, M. A.; Brennan, R. G.; Lu, P. Science 1996, 271, 1247.

121. Friedman, A. M.; Fischmann, T. O.; Steitz, T. A. Science 1995, 268, 1721.

122. Ptashne, M. A Genetic Switch; Cell Press & Blackwell Scientific Publications: Cambridge, MA, 1992, 2nd ed.

123. Müller–Hill, B. The lac Operon; Walter de Gruyter: New York, 1996.

124. Balaeff, A.; Koudella, C. R.; Mahadevan, L.; Schulten, K. Philos Trans R Soc Lond A 2004, 362, 1355.

125. Balaeff, A.; Mahadevan, L.; Schulten, K. Structure 2004, 12, 123.

126. The RCSB Protein Data Bank. http://www.rcsb.org/pdb.

127. Edelman, L. M.; Cheong, R.; Kahn, J. D. Biophys J 2003, 84, 1131.

128. Bhandarkar, M.; Budescu, G.; Humphrey, W.; Izaguirre, J. A.; Izrailev, S.; Kalé, L. V.; Kosztin, D.; Molnar, F.; Phillips, J. C.; Schulten, K. In Proceedings of the SCS International Conference on Web-Based Modeling and Simulation; Bruzzone, A. G.; Uchrmacher, A.; Page, E. H., Eds.; SCS International, San Francisco: San Francisco, CA, 1999, p. 242.